

1 *Bosio, G., Malinverno, E., Collareta, A., Di Celma, C., Gioncada, A., Parente, M., Berra, F., Marx,*  
2 *F.G., Vertino, A., Urbina, M. & Bianucci, G. (2019). Strontium Isotope Stratigraphy and the*  
3 *thermophilic fossil fauna from the middle Miocene of the East Pisco Basin (Peru). Journal of South*  
4 *American Earth Sciences, 102399.*

5 DOI: <https://doi.org/10.1016/j.jsames.2019.102399>

6

---

7 **Strontium Isotope Stratigraphy and the thermophilic fossil fauna from the middle Miocene of**  
8 **the East Pisco Basin (Peru)**

9

10 Giulia Bosio<sup>1,2\*</sup>, Elisa Malinverno<sup>2</sup>, Alberto Collareta<sup>1</sup>, Claudio Di Celma<sup>3</sup>, Anna Gioncada<sup>1</sup>,  
11 Mariano Parente<sup>4</sup>, Fabrizio Berra<sup>5</sup>, Felix G. Marx<sup>6,7,8</sup>, Agostina Vertino<sup>9</sup>, Mario Urbina<sup>10</sup>, Giovanni  
12 Bianucci<sup>1</sup>

13

14 <sup>1</sup> Dipartimento di Scienze della Terra, Università di Pisa, 56126 Pisa, Italy

15 <sup>2</sup> Dipartimento di Scienze dell’Ambiente e della Terra, Università degli Studi di Milano-Bicocca,  
16 20126 Milano, Italy

17 <sup>3</sup> Scuola di Scienze e Tecnologie, Università di Camerino, 62032 Camerino, Italy

18 <sup>4</sup> Dipartimento di Scienze della Terra, dell’Ambiente e delle Risorse, Università degli Studi di  
19 Napoli Federico II, 80126 Napoli, Italy

20 <sup>5</sup> Dipartimento di Scienze della Terra “Ardito Desio”, Università di Milano, 20126 Milano, Italy

21 <sup>6</sup> Directorate of Earth and History of Life, Royal Belgian Institute of Natural Sciences, 1000  
22 Brussels, Belgium

23 <sup>7</sup> School of Biological Sciences, Monash University, VIC 3800 Clayton, Victoria, Australia

24 <sup>8</sup> Palaeontology, Museums Victoria, VIC 3053 Melbourne, Victoria, Australia

25 <sup>9</sup> Department of Geology, Renard Centre of Marine Geology, Universiteit Gent, 9000 Ghent,  
26 Belgium

27 <sup>10</sup> Departamento de Paleontología de Vertebrados, Museo de Historia Natural, Universidad  
28 Nacional Mayor de San Marcos, Lima 1, Peru

29 \* *Corresponding author. E-mail address: giulia.bosio.giulia@gmail.com*

## 30 **Highlights**

- 31 - We applied Sr isotope dating to carbonates and phosphates from the East Pisco Basin
- 32 -  $^{87}\text{Sr}/^{86}\text{Sr}$  values date the lower Pisco strata (P0 sequence) to the middle Miocene
- 33 - Paleontological data indicate a warm water paleoenvironment for P0
- 34 - Our results suggest a middle-late Miocene strengthening of the Humboldt Current

35

## 36 **Abstract**

37 New age estimates obtained via Strontium Isotope ( $^{87}\text{Sr}/^{86}\text{Sr}$ ) Stratigraphy and new paleoclimatic  
38 data are here presented for the Miocene Chilcatay and Pisco formations exposed in the East Pisco  
39 Basin, an Andean forearc basin of southern Peru, which is renowned worldwide for its exceptional  
40 content of fossil marine vertebrates. Mollusk and barnacle shells, carbonate nodules, and shark teeth  
41 were collected along three stratigraphic sections for applying Strontium Isotope Stratigraphy on  
42 both carbonates and phosphates. To avoid diagenetic biases, mollusk and barnacle shells were  
43 analyzed in detail by means of optical and scanning electron microscopy, cathodoluminescence, and  
44 inductively coupled plasma-optical emission spectrometry, whereas only the enameloid from the  
45 best-preserved shark teeth was sampled. The obtained  $^{87}\text{Sr}/^{86}\text{Sr}$  ages confirm a late early Miocene  
46 (Burdigalian) age for the Chilcatay strata, and reveal middle Miocene (Langhian to Serravallian)  
47 ages for the lower Pisco unit (i.e., the P0 sequence) – a result that matches the relatively archaic  
48 aspect of its cetacean fossil assemblage. New and literature data about the fossil assemblage of the  
49 lower Pisco beds highlight the presence of several thermophilic invertebrates and vertebrates, thus  
50 suggesting a warm-water, tropical paleoenvironment for this middle Miocene sequence. Such a  
51 paleoenvironmental scenario recalls the warm conditions associated with the Chilcatay Formation,  
52 rather than the cooler setting inferred for the remainder of the Pisco Formation (i.e., the P1 and P2  
53 sequences). This pattern likely reflects the late Miocene trend of global cooling or a middle to early  
54 late Miocene strengthening of the Humboldt Current.

55

## 56 **Keywords**

57  $^{87}\text{Sr}/^{86}\text{Sr}$  stratigraphy, diagenesis evaluation, Miocene, mollusks, shark teeth, cetaceans

58

## 59 **1. Introduction**

60 The  $^{87}\text{Sr}/^{86}\text{Sr}$  ratio of Sr (strontium) isotopes dissolved in the global ocean has varied through the  
61 geological time (McArthur, 1994; McArthur et al., 2012). At the same time, the world's seas are  
62 homogeneous with respect to  $^{87}\text{Sr}/^{86}\text{Sr}$  ratio, and this is assumed for any geologic time (McArthur et  
63 al., 2012). Therefore, Sr isotope composition can be used for dating marine minerals and correlating

64 marine sedimentary successions worldwide (Faure and Mensing, 2005). Application of Strontium  
65 Isotope Stratigraphy (hereinafter: SIS) requires measurement of the Sr isotope ratio of minerals that  
66 precipitated from seawater and have not undergone diagenetic alteration of their original  $^{87}\text{Sr}/^{86}\text{Sr}$   
67 value (McArthur et al., 2012). Some intervals of geological time, such as the Miocene, are  
68 particularly favorable for implementation of SIS because they display high rates of change of the  
69  $^{87}\text{Sr}/^{86}\text{Sr}$  value and a narrow error band on the empirically defined reference curve (McArthur et al.,  
70 2012), which allow for high-resolution age estimates.

71 The Miocene Chilcatay and Pisco formations exposed in the East Pisco Basin of southern Peru  
72 are renowned for their exceptional fossil assemblage, comprising cetaceans, seals, sharks, rays,  
73 crocodiles, turtles, seabirds, and bony fishes (e.g., Bianucci et al., 2015, 2016a, b, c, 2018a, b;  
74 Lambert et al., 2014, 2015b, 2017a, b, 2018; Landini et al., 2017a, b, 2019; Marx et al., 2017a, b;  
75 Gioncada et al., 2018b) as well as marine invertebrates (e.g., DeVries and Frassinetti, 2003;  
76 DeVries et al., 2006; DeVries, 2016; Coletti et al., 2018, in press; Collareta et al., 2019). In  
77 particular, the fossil record of the Pisco Formation is outstanding in terms of both abundance and  
78 preservation state of the vertebrate remains. Examples of exceptionally preserved fossil vertebrate  
79 specimens from the Pisco strata exposed in the East Pisco Basin include phosphatized baleen  
80 bristles and plates of mysticete whales (Brand et al., 2004; Esperante et al., 2008; Gioncada et al.,  
81 2016; Marx et al., 2017a), stomach contents and regurgitations of mysticete and odontocete  
82 cetaceans (Collareta et al., 2015; Lambert et al., 2015a), and phosphatized skeletons of cartilaginous  
83 fishes such as sharks (Collareta et al., 2017).

84 For interpreting this extraordinary paleontological heritage and enhancing its scientific  
85 significance, its placement in a robust stratigraphic context supported by reliable age estimates is  
86 crucial. Recent work established a chronostratigraphic framework based on  $^{39}\text{Ar}$ - $^{40}\text{Ar}$  dating,  
87 tephrostratigraphy and biostratigraphy, which dates the Chilcatay Formation to the early Miocene  
88 and the upper sequences of the Pisco Formation to the late Miocene, respectively (Di Celma et al.,  
89 2017, 2018a, b; Gariboldi et al., 2017; Bosio et al., 2019, in press). The seemingly large temporal  
90 gap between these two units is striking, but is almost certainly an overestimate caused by a lack of  
91 datable ash layers and microfossils from the lowermost portion of the Pisco Formation (the P0  
92 sequence). Previous studies remarked on the significantly archaic aspect of the cetacean fauna from  
93 this layer (Di Celma et al. 2017; Marx et al. 2017b), but were unable to draw definitive conclusions  
94 as to its age. The peculiar faunal changes that characterize this sequence (Di Celma et al., 2017)  
95 make the dating of these strata an issue of prime importance for the ongoing paleontological studies  
96 on the Miocene fossil content of the East Pisco Basin.

97 Here, we present the first attempt to date the lower Pisco beds by means of SIS. Mollusk (i.e.,  
98 ostreids and pectinids) and barnacle shells, diagenetic cements, bulk sediment samples, and shark  
99 teeth were collected to apply this method to both carbonates and phosphates. Several samples from  
100 the age-constrained Ct1 sequence of the Chilcatay Formation were dated for checking the reliability  
101 of the Sr results in the study areas. The preservation state of the invertebrate remains was  
102 preliminary addressed via petrographic, morphological, chemical, and cathodoluminescence  
103 analyses in order to quantify the extent of diagenetic alteration and to assess whether the shells were  
104 structurally and chemically pristine. Sr isotope ratios were elaborated with the LOWESS Table 5  
105 made for the GTS2012 timescale (McArthur et al., 2012) and SIS ages were obtained.

106 Furthermore, we investigated the faunal assemblages of both fossil invertebrates and vertebrates  
107 for reconstructing the environmental and paleoclimatic significance of the P0 sequence in the light  
108 of our age estimates. Having been deposited in a key time interval that saw first-order changes of  
109 the climate and oceanographic system at both the global scale (e.g., the Middle Miocene Climatic  
110 Optimum and the Middle Miocene Climatic Transition) and the regional scale (e.g., the emergence  
111 of the modern upwelling regime along the Pacific margin of South America), the P0 sequence and  
112 its newly dated fossil content represent indeed crucial elements for reconstructing the mode and  
113 tempo of the major Miocene environmental shift episodes off the coast of Peru – the current  
114 location of the outstandingly productive Humboldt Current (Penven et al., 2005).

115

## 116 **2. Geological and paleontological framework**

117 The East Pisco Basin is one of the elongated extensional/pull-apart sedimentary basins along the  
118 composite transform-convergent Peruvian margin (e.g., Thornburg and Kulm, 1981; Kulm et al.,  
119 1982; Dunbar et al., 1990; León et al., 2008; Zúñiga-Rivero et al., 2010) (Fig. 1A). Its emersion and  
120 subaerial exposure is due to the subduction of the nearby Nazca Ridge, a region of topographically  
121 high oceanic crust impinging on the Peru-Chile trench (Pilger, 1981; Hsu, 1992; Macharé and  
122 Ortlieb, 1992; Hampel, 2002). The basin fill comprises, in stratigraphic order, the Eocene Caballas  
123 and Paracas formations, the upper Eocene to lower Oligocene Otuma Formation, and the largely  
124 Miocene Chilcatay and Pisco formations (Dunbar et al., 1990; DeVries, 1998, 2017; DeVries et al.,  
125 2017; DeVries and Jud, 2018) (Fig. 1C). These units are bounded by regionally extensive  
126 unconformities and are also internally divided by less pronounced intraformational unconformities  
127 (DeVries, 1998; Di Celma et al., 2017, 2018a, b). As such, this succession can be subdivided using  
128 both a lithostratigraphic and an allostratigraphic approach (North American Commission on  
129 Stratigraphic Nomenclature [NACSN], 2005). In the present paper, we refer to the formations as  
130 “composite sequences” and to their internal informal units as “sequences”.

131 During deposition of the Chilcatay and Pisco formations, the East Pisco Basin was a semi-  
132 enclosed, shallow-marine bay, structured along a latitudinal depth gradient, and sheltered seawards  
133 by a longshore chain of crystalline basement islands (Fig. 1B) (Marocco and Muizon, 1988;  
134 DeVries and Jud, 2018; Bianucci et al., 2018b).

135 The Chilcatay Formation was deposited during the late early Miocene, between 19 and 17 Ma  
136 (Burdigalian) (Belia et al. 2019; Di Celma et al., 2018b; Bosio et al., in press). It is composed of  
137 two distinct sequences, namely, Ct1 and Ct2 (Di Celma et al., 2018b, 2019) (Fig. 1C). At Ullujaya  
138 (14°34'59"S; 75°38'27"W) and Roca Negra (14°39'04"S; 75°38'54"W), two localities along the  
139 western side of the Ica River (Fig. 2A, 3A, B), the lower sequence (Ct1) of the Chilcatay Formation  
140 consists of massive sandstones and conglomerates with boulder-sized clasts at the bottom (*Ct1c*  
141 facies association), followed by medium- to fine-grained sandstones alternating with conglomerate  
142 beds (*Ct1a*), and clinobedded coarse-grained calcirudites at the top (*Ct1b*) (Di Celma et al., 2018b,  
143 2019). These facies associations record deposition in the shoreface, offshore, and on a mixed  
144 siliciclastic-carbonate subaqueous delta, respectively (Di Celma et al., 2019), and suggest a semi-  
145 protected embayment associated with both a river mouth and the open ocean (Bianucci et al.,  
146 2018b). The invertebrate fossil assemblage of the Chilcatay strata exposed at the study sites  
147 comprises mollusks, barnacles, serpulids and echinids (Di Celma et al., 2018b, 2019). Bivalves are  
148 represented by ostreids, pectinids and venerids. Barnacles mainly belong to three taxa, with  
149 *Austromegabalanus carrioli* being the most abundant (Coletti et al., 2018, in press; Collareta et al.,  
150 2019). The vertebrate fossil assemblage is dominated by toothed cetaceans (Odontoceti), including  
151 kentriodontids (*Kentriodon* sp.), squalodelphinids (*Notocetus vanbenedeni* and *Huaridelphis*  
152 *raimondii*), physeteroids (sperm whales), and the eurhinodelphinid-like *Chilcacetus* (Bianucci et al.,  
153 2015, 2018b; Lambert et al., 2014, 2015b; Di Celma et al., 2018b, 2019). In addition, there are sea  
154 turtles (large-sized indeterminate dermochelyids), bony fishes and elasmobranchs, with abundant  
155 juvenile teeth of the bronze shark *Carcharhinus brachyurus* and the extinct lamniform  
156 *Cosmopolitodus hastalis*. Overall, the fossil assemblage points to a coastal community dominated  
157 by warm-water mesopredators (Bianucci et al., 2018b).

158 The Pisco Formation is composed of three fining-upward sequences, designated P0, P1, and P2  
159 from oldest to youngest, which are divided by three unconformities, named PE0.0, PE0.1, PE0.2,  
160 respectively (Fig. 1C). Each unit, representing a transgressive cycle, recorded deposition in  
161 shoreface (sandstones) and in offshore (siltstones/diatomaceous siltstones) settings. The time of  
162 deposition of the P1 and P2 sequences is late Miocene and is well-constrained between 9.5 Ma and  
163 8.6 Ma, and between 8.4 and 6.7 Ma, respectively (Gariboldi et al., 2017; Bosio et al., in press).  
164 Due to the lack of tephra layers and microfossils, the depositional age of the lower unit, P0, is to

165 date very poorly constrained between 18 and 9.5 Ma (Di Celma et al., 2017; Bosio et al., in press).  
166 Note, however, that DeVries and Jud (2018) previously proposed an early–middle Miocene age for  
167 the lower portion of the Pisco Formation (including P0), based on a series of diatom samples  
168 analyzed by H. Schrader in the 1980s. The P0 strata of the Pisco Formation reach their maximum  
169 thickness (about 40 m) at the locality of Cerro Submarino (14°34'38"S; 75°39'51"W) (Fig. 3D).  
170 This unit is mostly composed of fine- to very coarse-grained, cross-stratified, fossil-rich sandstones,  
171 suggesting a very nearshore environment. The fossil invertebrate assemblage of P0 is dominated by  
172 mollusks, with barnacles being less common. Mollusks are mostly represented by bivalves and  
173 primarily include *Chionopsis* spp. and *Dosinia ponderosa*, but *Miltha* cf. *vidali* and ostreids are also  
174 present (Di Celma et al., 2017). Vertebrates are abundant, but less studied than those from the  
175 underlying Chilcatay strata. Baleen whales (Cetacea: Mysticeti) dominate the assemblage and are  
176 represented by i) a large-sized stem balaenopteroid, *Pelocetus* sp. (Bianucci et al., 2019); ii) the  
177 archaic cetotheriid *Tiucetus rosae*, previously described from the southeastern locality of Santa  
178 Rosa (Marx et al., 2017b); and iii) a third form, previously identified as a cetotheriid (Di Celma et  
179 al., 2017), but here more conservatively reinterpreted as an indeterminate plicogulan (i.e., a crown  
180 mysticete more closely related to extant rorquals than to extant right whales). Toothed whales  
181 include at least one physeteroid and two kentriodontid-like delphinoids. In addition, there are  
182 fragmentary fossils of chelonoid turtles and longirostrine crocodylians, and a single bird specimen  
183 representing an indeterminate pelagornithid (Di Celma et al., 2017). Shark and ray teeth are  
184 relatively common and include, among others, *Carcharocles megalodon*, *Cosmopolitodus hastalis*,  
185 *Isurus oxyrinchus*, and myliobatids (eagle rays) (Di Celma et al., 2017).

186

### 187 3. Material and Methods

#### 188 3.1. Study area and sample collection

189 The study area is settled in the Ica Desert, at the localities of Roca Negra (14°39'04"S;  
190 75°38'54"W) and Ullujaya (14°34'59"S; 75°38'27"W), where the Chilcatay Formation crops out (Di  
191 Celma et al., 2018b, 2019; Bianucci et al., 2018b), and Cerro Submarino (14°34'38"S;  
192 75°39'51"W), where P0 displays its maximum thickness (40 m) (Fig. 2, 3).

193 From 2015 and during five successive field campaigns, the Chilcatay and Pisco outcrops at the  
194 localities of Roca Negra, Ullujaya, and Cerro Submarino were investigated in detail for fossil  
195 vertebrates and macro-invertebrates by means of systematic surface prospecting. Preliminary  
196 identifications of the surveyed fossil specimens were made in the field. A few highly significant  
197 specimens, including representatives of the thermophilic taxa reported herein, were collected and



198 deposited in the Museo de Historia Natural de la Universidad Nacional Mayor de San Marcos  
199 (MUSM) in Lima for preparation and study.

200 Samples collected for applying the SIS were carbonates (invertebrate shells, diagenetic cements)  
201 and phosphates (shark teeth). For the Sr isotope analyses, shark tooth fluorapatite and low-Mg  
202 calcite shells were preferred, as low-Mg calcite is more stable, more resistant to diagenesis and less  
203 soluble than other carbonates (Brand, 1991; Steuber, 2003). Mollusks (i.e., ostreids and pectinids)  
204 and barnacles, shark teeth, and bulk and cement samples were collected along the measured section  
205 of the well-dated Chilcatay Formation at Roca Negra and Ullujaya, as well as from the undated P0  
206 deposits at Cerro Submarino (Fig. 2, 3). Different horizons were selected at each locality (Fig. 3, C)  
207 and, for each level, several carbonate shells were sampled, usually from different organisms (e.g.,  
208 oysters, pectinids, and barnacles). Some bulk and cement samples were also analyzed for better  
209 understanding the diagenetic path and its effects on  $^{87}\text{Sr}/^{86}\text{Sr}$  values.

210

### 211 3.2. *Optical microscopy (OM), scanning electron microscopy (SEM), and cathodoluminescence*

212 Diagenetic processes or weathering could modify the pristine  $^{87}\text{Sr}/^{86}\text{Sr}$  ratio of carbonate and  
213 phosphate marine minerals, providing wrong ages of mineral formation (Scasso et al., 2001; Brand  
214 et al., 2012; Ullmann and Korte, 2015). Therefore, their identification is critical for evaluating the  
215 reliability of the  $^{87}\text{Sr}/^{86}\text{Sr}$  ratio, which is suitable for SIS only when post-depositional alterations can  
216 be excluded. With the aim of evaluating the impacts of diagenesis and weathering on shells,  
217 mollusk and barnacle samples from both the Chilcatay and Pisco formations have been prepared for  
218 realizing thin sections. Petrographic analyses of polished thin sections were carried out through  
219 Leica and Olympus optical microscopes. A SEM-EDS Tescan VEGA TS Univac 5136XM was  
220 used at the Department of Earth and Environmental Sciences of the Università degli Studi di  
221 Milano-Bicocca for petrographic and morphological observations, as well as for checking evidence  
222 of dissolution in the structure of the selected shells. Cathodoluminescence was performed using a  
223 CITL Optical Cathodoluminoscope at the Department of Earth Science "Ardito Desio" of the  
224 Università degli Studi di Milano, operated at about 14kV accelerating voltage and 0.5 mA gun  
225 current intensity. Cathodoluminescence observations permitted the identification of different  
226 carbonate generations, as well as of recrystallized portions of the shells (Barbin, 2013; Ullman and  
227 Korte, 2015).

228 Pristine shells were chosen for the age calculation, whereas shells showing a recrystallized  
229 and/or dissolved texture under both the optical and the electron microscope and a high  
230 luminescence under the cathodoluminoscope were discarded. Some recrystallized materials were  
231 also selected for  $^{87}\text{Sr}/^{86}\text{Sr}$  analyses, for understanding how diagenesis changed the Sr ratio (i.e.,

232 diagenesis path) (Steuber, 2003). Regarding shark teeth, samples were taken from the outer  
233 enameloid layer (Enax et al., 2014), avoiding dentine, which is generally more porous and  
234 susceptible to diagenetic alteration than enameloid (Becker et al., 2008). Sr isotope measurement on  
235 the enameloid portion of shark teeth has proven to provide reliable age estimates (Becker et al.,  
236 2008; Harrell et al., 2016).

237 After the preliminary analyses, fifteen samples were selected from the Ct1 sequence of the  
238 Chilcatay Formation, whereas eight samples were selected from the P0 sequence of the Pisco  
239 Formation (Table 1).

240

### 241 3.3. Compositional and strontium isotope analyses

242 After microscopic investigations, the selected pristine mollusk shells and well-preserved  
243 barnacle sheaths were carefully cleaned through an ultrasonic bath in distilled water. They were  
244 bored with a Dremel micro-drill to obtain shell powder from the diagenetically unaltered portion.  
245 After an ultrasonic bath in distilled water, the selected shark teeth were also scraped as powder of  
246 their unaltered, non-porous enameloid was collected with the micro-drill. About 10-50 mg of each  
247 sample were collected for inductively coupled plasma-optical emission spectroscopy (ICP-OES)  
248 and  $^{87}\text{Sr}/^{86}\text{Sr}$  analyses, taking care to avoid contaminations.

249 ICP-OES and  $^{87}\text{Sr}/^{86}\text{Sr}$  analyses were made at the Institute für Geologie, Mineralogie und  
250 Geophysik of the Ruhr-Universität of Bochum. ICP-OES analyses were made with a Thermo Fisher  
251 Scientific iCAP 6500 DUO spectrometer for analyzing the concentrations of Sr, Ca (calcium), Mg  
252 (magnesium), Fe (iron), and Mn (manganese).

253  $^{87}\text{Sr}/^{86}\text{Sr}$  ratios were determined with a TIMS Finnigan MAT 262 solid source mass spectrometer  
254 with seven collectors, using a dynamic (peak-hopping) mode of measurement. The cut-off limit for  
255 a strontium run was an error of  $\pm 2\sigma \leq 5 \times 10^{-6}$  for the  $^{87}\text{Sr}/^{86}\text{Sr}$  ratio, with 100–200 ratios per run  
256 (typical duration: 110 ratios, lasting 2 h 15 min, plus the filament heating time). Two standards –  
257 NIST NBS 987 and USGS EN-1 – were used to calibrate the analysis. NIST NBS 987 was loaded  
258 directly onto the filament, to confirm the stability of the mass spectrometer. USGS EN-1, a powder  
259 derived from a modern *Tridacna* shell, underwent the same procedure as the other carbonate  
260 samples, to ensure the reproducibility of the entire analytical process. Thirty-four analyses of NIST  
261 NBS 987 resulted in a mean of  $0.710240 \pm 0.000023$  ( $2\sigma$ ), while 24 analyses of USGS EN-1  
262 yielded  $0.709153 \pm 0.000019$  ( $2\sigma$ ). No Rb (rubidium) correction was applied, but Rb was  
263 nonetheless monitored during the entire run. When Rb levels exceeded the detection limit, the result  
264 was discarded and the measurement repeated.



265 The results of the  $^{87}\text{Sr}/^{86}\text{Sr}$  analyses were corrected for the difference between the USGS EN-1  
266 value used for the compilation of the reference curve (McArthur et al., 2012) and the USGS EN-1  
267 Bochum mean value, and then converted into ages using the LOWESS Table 5, which is tied to the  
268 GTS2012 timescale (McArthur et al., 2012). The latter is still incomplete, therefore the results were  
269 rounded off to the nearest value. Following the method described by Frijia et al. (2015), when more  
270 than one sample was analyzed for a single layer, a mean  $^{87}\text{Sr}/^{86}\text{Sr}$  value was calculated. The  
271 uncertainty for each stratigraphic level was calculated as 2 s.e. (i.e., standard error) from the  
272 standard deviation of the mean.

273

## 274 **4. Results**

### 275 *4.1. Diagenesis evaluation for SIS analyses*

276 The Chilcatay and Pisco formations present notably divergent patterns of carbonate preservation.  
277 In the Chilcatay Formation, fossil invertebrates are well-preserved and retain their pristine calcitic  
278 shells. In contrast, in the Pisco Formation, calcitic shells are only present in the P0 sequence, where  
279 examples of calcite recrystallization also occur, but not in P1 and P2, where mollusks are only  
280 preserved as casts (Di Celma et al., 2017). For these reasons, SIS could only be applied in the Ct1  
281 and P0 sequences, once some caveats have been taken into account, such as in-depth petrographic  
282 and chemical analyses of the samples.

283 At the macroscale, all of the bivalves selected for Sr analyses from both the units appear well-  
284 preserved and composed of calcite. The oysters (Fig. 4A) are usually incised by attachment traces  
285 by sponges and/or drill holes due to the predatory action of carnivorous gastropods; in several cases,  
286 they preserve layers of unaltered nacre. The pectinids (Fig. 4B) are also well-preserved, with small  
287 borings and some barnacle attachment traces (*Anellusichnus*; Santos et al., 2005). By contrast, the  
288 barnacles (Fig. 4C) generally display obvious signs of abrasion and lack their opercula; the best-  
289 preserved and less porous portion of the shell is often constituted by the sheath, the thickened upper  
290 part of the inner wall (see Fig. 4C). Shark teeth selected for Sr analyses are moderately- to well-  
291 preserved; although two shark teeth show a breakage surface in their root, they all have an intact  
292 thin layer of enameloid that surrounds the pulp cavity and covers the surface of the tooth crown  
293 (Fig. 4D).

294 Microscopically, the best-preserved pectinids and ostreids are characterized by foliated and  
295 prismatic calcite, respectively (Fig. 5A, C) (Cox et al., 1971). Both also have a low, homogeneous  
296 luminescence, suggesting little or no diagenesis (Fig. 5B, D). Nevertheless, some of the analyzed  
297 ostreids also have layers that are luminescent, documenting diagenetic modifications. Microborings  
298 filled by luminescent calcite or terrigenous sediments, can be observed (Fig. 5C, D). These infills

299 must be avoided during sampling for Sr isotope analyses, because they could have non-pristine Sr  
300 ratio. As reported also by Crippa et al. (2016), fossil ostreids occasionally exhibit layers of sparry  
301 calcite replacing the pristine aragonitic layers (i.e., myostracum) or filling the chambers once  
302 permeated by organic matter (Fig. 5E, F). All those specimens that present similar features were  
303 discarded from the Sr analyses. Several oysters from the Ct1 and P0 sequences that exhibit a  
304 generally low luminescence have discrete luminescent layers that appear pristine and prismatic. For  
305 explaining this feature, which has also been documented in modern oysters, Barbin (1991, 2013)  
306 argued that luminescence may not be always a convincing indicator of diagenetic alteration for  
307 oysters, because the absorption of  $Mn^{2+}$  by benthic organisms depends on various factors, such as  
308 growth rate, ontogeny, bathymetry, salinity, and redox conditions. To minimize the risk of  
309 diagenetic bias, we conservatively discarded all the ostreid samples with diffuse microborings,  
310 sparry calcite, or displaying high and/or heterogeneous luminescence. By contrast, the best-  
311 preserved barnacles are characterized by low luminescence throughout the less porous portion of  
312 the wall, but high luminescence characterized the parietal tubes, which are normally filled with  
313 secondary calcite (Fig. 5G, H). We carefully avoided to contact the parietal tubes during sampling  
314 of the barnacle shells for the strontium analysis.

315 Secondary electron (SE) images confirmed the presence of alternating prismatic and sparry  
316 calcite layers in some ostreid specimens (Fig. 6A, B) that were hence discarded. Other specimens  
317 either retain a pristine prismatic layer (Fig. 6C) or show clear signs of alteration such as obliteration  
318 of the pristine prismatic texture (very irregular or dissolved) and widespread, pervasive holes (Fig.  
319 6D). Again, specimens exhibiting obvious evidence of diagenesis were discarded.

320 ICP-OES analysis is useful for measuring the Fe, Mn, Mg, and Sr concentrations, which in turn  
321 can be informative in terms of diagenetic imprint on carbonates. Usually, the Fe and Mn contents of  
322 carbonates increase during the diagenetic processes; on the contrary, the Mg and Sr contents  
323 generally decrease during diagenesis (Brand and Veizer, 1980; McArthur, 1994; Steuber, 1999).  
324 Fixed or static limits for Fe, Mn and Sr content have been proposed by several authors to  
325 discriminate between pristine and altered biotic low-Mg calcite of fossil shells (see Ullmann and  
326 Korte, 2015 for a recent review). However, this approach totally ignores natural variation due to  
327 spatial and temporal differences (Brand et al., 2011; Ullmann and Korte, 2015). For this reason,  
328 following the approach of Brand et al. (2012), we evaluated separately each stratigraphic horizon,  
329 comparing the chemical composition of different coeval components (i.e. optically well preserved  
330 shells, recrystallized shells, cemented bulk sediment enclosing or encrusting the shells) to select the  
331 best preserved material. In Figure 7A, the low Sr content of cement and bulk samples indicates a  
332 decrease in Sr during diagenesis, as reported by Frijia and Parente (2008) for diagenetically altered

333 marine carbonates, coupled with a decrease of the  $^{87}\text{Sr}/^{86}\text{Sr}$  value. The latter trend is opposite to  
334 what is normal observed in diagenetically altered carbonates, when the interaction of the diagenetic  
335 fluids with siliciclastic rocks generally results in more radiogenic Sr isotope values (McArthur,  
336 1994). The decrease of the Sr ratio in the diagenetically altered calcite of the studied successions  
337 can be due to the pre-Miocene seawater-derived brine circulating within the sedimentary sequence,  
338 as reported by Gioncada et al. (2018a). This decrease of the Sr isotope ratio from pristine to  
339 diagenetic calcite confers older Sr ages to the diagenetically altered samples. The abundance of Fe  
340 and Mn in the diagenetic samples (see Fig. 7B, C, D) conforms to the expected pattern of increasing  
341 Fe and Mn concentration during diagenesis. The above reconstruction of the diagenetic paths helps  
342 in assessing the preservation of each sample. Indeed, samples displaying the same degree of  
343 morphological preservation but higher concentrations of Sr and lower concentrations of Fe and Mn  
344 might be considered as retaining the pristine Sr isotope ratio of seawater.

345

#### 346 4.2. Strontium Isotope Stratigraphy of the *Ct1* sequence

347 After discarding all those shells that may have been affected by post-depositional modifications,  
348 fifteen samples from the *Ct1* sequence of the Chilcatay Formation (Ullujaya and Roca Negra) were  
349 selected for  $^{87}\text{Sr}/^{86}\text{Sr}$  analysis (Table 1). From each locality, Sr isotope analyses of different well-  
350 preserved shells yielded similar Sr isotope values. The internal consistency of the Sr isotope ratios  
351 of different samples from the same stratigraphic level can be regarded as a strong argument  
352 supporting the preservation of the original seawater  $^{87}\text{Sr}/^{86}\text{Sr}$  value (McArthur et al., 1994; Steuber,  
353 2003).

354 At Roca Negra, we sampled three well-preserved oysters (PN-OST, PN-GIO1, PN-GIO2) from  
355 the *Ct1c* facies association. The three specimens came from a single bed (PN Oyster bed; Fig. 3C)  
356 close to the base of the formation, ca. seven meters above an ash layer (PN-T2) dated to  $19.25 \pm$   
357  $0.05$  Ma by Bosio et al. (in press). Sr isotope analyses give similar  $^{87}\text{Sr}/^{86}\text{Sr}$  results (Table 1) and the  
358 mean value gives a preferred age of 18.50 with a range of uncertainty spanning between 18.85 and  
359 18.15 Ma (Table 2).

360 At Ullujaya, we sampled 12 specimens from the *Ct1a* facies association, between a basal ash  
361 layer (UJA-T35) dated to  $19.00 \pm 0.28$  Ma by Bosio et al. (in press) and a second ash layer in the  
362 overlying *Ct2b* facies association (SOT-T3; Fig. 3C) dated to  $18.02 \pm 0.07$  Ma by Di Celma et al.  
363 (2018b).

364 Three samples – a barnacle sheath (UL-LIVa), composite sample of two pectinids (UL-LIVb),  
365 and a further, single pectinid (UL-LIVc) – were chosen from a layer 9 m above the base of the  
366 measured section (hereafter: abs), named “mollusk- and barnacle-rich horizon” by Collareta et al.

367 (2019) (Fig. 3C). The mean value of the  $^{87}\text{Sr}/^{86}\text{Sr}$  values gives again a preferred age of 18.50 Ma  
368 and an uncertainty that ranges from 18.60 to 18.40 Ma for this horizon (Table 2).

369 At 17 m abs, in occurrence of the key bed C (KbC of Di Celma et al., 2018b) (Fig. 3C), naacre  
370 layers of two well-preserved oysters were selected (UJA-LIVC1, UJA-LIVC3) together with a  
371 barnacle sheath (UJA-LIVC4) (Table 1). In addition, a sample of the cemented bulk sediment from  
372 the outer part of an oyster shell was also analyzed (UJA-LIVC2). Considering only the ages from  
373 the pristine shells, we obtained similar  $^{87}\text{Sr}/^{86}\text{Sr}$  values and Burdigalian ages (see Tables 1, 2). The  
374 bulk sample UJA-LIVC2 shows a lower value of  $^{87}\text{Sr}/^{86}\text{Sr}$  ratio and gives older ages (i.e., 21.45–  
375 21.00 Ma), suggesting an ageing effect caused by diagenesis, as discussed above. The age range of  
376 the key bed C is thus comprised between 18.50 and 18.10 Ma, with a preferred age of 18.30 Ma  
377 (Table 2). The SIS age of this bed is apparently younger than that of the bed below (i.e., the  
378 mollusk- and barnacle-rich horizon), dated at ca. 18.50 Ma, although the two obtained age ranges  
379 are still largely overlapping.

380 Three samples were selected for the UL-D4 bed, a carbonate-rich horizon located 25 m abs (see  
381 Fig. 3C): UL-D4a, from prismatic layers of an oyster; UL-D4b, from a barnacle sheath; UL-D4c,  
382 the bulk sediment cemented within the same barnacle shell (Table 1). The bulk sample, UL-D4c,  
383 exhibits a relatively low  $^{87}\text{Sr}/^{86}\text{Sr}$  value and, consequently, a relatively older age value (i.e., 19.60–  
384 19.20 Ma), indicating that diagenesis had an ageing effect on the shells also in this bed. The shell  
385 samples from the UL-D4 bed did not return consistent values of  $^{87}\text{Sr}/^{86}\text{Sr}$  (see Supplementary  
386 Material) and they were discarded from the age determination.

387 Finally, at 30 m abs, we took two samples (UJA-2a and UJA-2b) from different layers of a single  
388 oyster shell, collected from key bed B of Di Celma et al. (2018b) (Fig. 3C). The mean  $^{87}\text{Sr}/^{86}\text{Sr}$   
389 value provides a preferred age of 18.30 Ma for the key bed B, with a maximum age of 18.60 Ma  
390 and a minimum age of 18.00 Ma, in agreement with the levels dated below (Table 2).

391 The  $^{87}\text{Sr}/^{86}\text{Sr}$  ages calculated for each bed give a Burdigalian age for the Ct1 sequence of the  
392 Chilcatay Formation. The time resolution of the SIS method is not sufficient to discriminate the age  
393 of these closely spaced horizons. However, the preferred ages of the sampled levels tend to be  
394 younger according to the stratigraphy.

395

#### 396 4.3. Strontium Isotope Stratigraphy of the P0 sequence

397 Carbonates from the P0 sequence are poorly preserved, resulting in just five samples from a ~10  
398 m-thick stratigraphic section located north of Cerro Submarino (Fig. 3D). Given the scarcity of  
399 suitable carbonate samples, we also collected samples from well-preserved shark teeth  
400 (phosphates). They show  $^{87}\text{Sr}/^{86}\text{Sr}$  values that are consistent with those of the pristine carbonate

401 samples (see Fig. 7, Table 1). Taking also into account the limited thickness of the P0 deposits  
402 exposed at Cerro Submarino, we considered all the collected samples as belonging to a single level  
403 and we calculated a unique  $^{87}\text{Sr}/^{86}\text{Sr}$  age starting from five different samples.

404 Three shark teeth were chosen from the lower portion of the P0 sequence, a few meters above  
405 the PE0.0 unconformity, in the plain northward of Cerro Submarino, here informally called “Tooth  
406 plain” (see Fig. 3D). Of the analyzed teeth, Tooth 1 is a lower anterolateral tooth of *Cosmopolitodus*  
407 *hastalis*, Tooth 2 is an upper tooth of the same species (Fig. 4D), and Tooth 3 is a lower tooth of  
408 *Isurus oxyrinchus* (see Table 1). The three resulting  $^{87}\text{Sr}/^{86}\text{Sr}$  values are slightly different from each  
409 other, but there are no morphological or chemical reasons to prefer one tooth over another and all  
410 these samples were selected for the final age calculation.

411 A few meters above the PE0.0 unconformity, a calcite nodule from within a baleen whale  
412 mandible (SUB-2, Table 1) was first selected following the hypothesis of precipitation during early  
413 diagenesis, similarly to what hypothesized for the dolomite nodules found inside bone cavities in  
414 the Pisco Formation (Gariboldi et al., 2015; Gioncada et al., 2016). However, SUB-2 has a very low  
415  $^{87}\text{Sr}/^{86}\text{Sr}$  value similar to the late diagenetic cements, suggesting a late diagenetic imprint of this  
416 nodule, and therefore it was discarded. Close to this sample, an oyster was collected (SUB-5, Fig.  
417 3D), and the thin nacre layers were drilled, giving an  $^{87}\text{Sr}/^{86}\text{Sr}$  value similar to those of the shark  
418 teeth. Finally, a few meters above, three samples were selected from level SUB-8bis (see Fig. 3D):  
419 one from the presumably pristinely preserved sheath of a barnacle (SUB-8bis1), one from the bulk  
420 sediment cemented inside the same barnacle shell (SUB-8bis2), and the last one from a completely  
421 recrystallized shell of a bivalve (SUB-8bis3) (Table 1). The samples from the bulk and the  
422 recrystallized bivalve indicate that, as in the Ct1 sequence, diagenesis resulted in a substantial  
423 reduction of the  $^{87}\text{Sr}/^{86}\text{Sr}$  value and a consequent increase of the calculated ages. In turn, the pristine  
424 calcite of the barnacle sheath shows an  $^{87}\text{Sr}/^{86}\text{Sr}$  value similar to the other pristine samples and was  
425 considered for the final age calculation.

426 Discarding samples affected by diagenesis, a mean  $^{87}\text{Sr}/^{86}\text{Sr}$  value can be calculated starting  
427 from 5 samples collected from the lower part of the P0 sequence. Together, the three shark teeth,  
428 SUB-5, and SUB8bis1 result in a mean age of 13.45 Ma, with an uncertainty time range spanning  
429 between 14.80 and 12.45 Ma. Consequently, by means of SIS, the P0 sequence can be placed in the  
430 Langhian–Serravallian (Table 2). The age of the P0 sequence is now resolved, but poorly  
431 constrained because of the scarcity of well-preserved specimens (allowing for just a few dated  
432 samples) and the intrinsic limits of the SIS method.

433

434 *4.4. Thermophilic invertebrates and vertebrates from the P0 sequence*

435 The thermophilic fossils identified from the P0 strata exposed in the vicinities of Cerro  
436 Submarino include members of both the invertebrate and vertebrate assemblages (Fig. 8).

437 Among the invertebrates, three cypraeid specimens could be identified as belonging to  
438 *Muracypraea ormenoi*, an extinct species that has been interpreted as a thermophilic taxon that  
439 shared the environmental and climatic preferences of extant *Muracypraea mus* (DeVries et al.,  
440 2006). Although the holotype of *M. ormenoi* was collected from Chilcatay beds, another specimen  
441 was reported by DeVries et al. (2006) from undifferentiated strata of the Pisco Formation in the  
442 vicinities of Cerro Submarino, where the P0 strata are mostly exposed (Di Celma et al., 2017,  
443 2018a). Unfortunately, the poor preservation state of the inner mold observed by us does not allow  
444 an unambiguous identification of these cypraeid specimens at the genus and species levels (see Fig.  
445 8A–C). A specimen of the gastropod *Ficus* cf. *distans* was also found in these strata (personal  
446 communication by T.J. DeVries, in Di Celma et al., 2017); according to DeVries and Frassinetti  
447 (2003) and Nielsen and Glodny (2009), *Ficus distans* should be regarded as a thermophilic member  
448 of a generally warm-water genus. Seven specimens belonging to the family Architectonicidae were  
449 also found (see Fig. 8H, I, J). Architectonicids were considered by Nielsen and Frassinetti (2007) as  
450 tropical and subtropical gastropods. Finally, the P0 invertebrate assemblage from the Cerro  
451 Submarino area includes the only known coral occurrence from the East Pisco Basin, reported in  
452 this paper for the first time. The single examined specimen consists of several tiny corallites (up to  
453 4.5 mm in calicular diameter) settled on two large barnacle shells (Fig. 8F, G). The distal part of the  
454 corallites is badly preserved, however their size, shape, septal number, septal arrangement, and  
455 stolon-like connections allow us to ascribe them to a colony of the tropical to warm temperate  
456 family Rhizangidae (Cairns et al., 2005). High affinities with the genus *Culicia* have been noted,  
457 but further (better preserved) specimens must be analyzed to confirm the genus-level identification.

458 With respect to the vertebrates, teeth and dermal spines belonging to various taxa of more or less  
459 thermophilic cartilaginous fishes have been collected from the studied P0 exposures. The  
460 elasmobranch assemblage includes abundant teeth of the requiem shark *Carcharhinus*, among  
461 which *Carcharhinus brachyurus* and *Carcharhinus* cf. *leucas* stand out. Most extant species of  
462 *Carcharhinus* are confined today to warm-temperate to tropical waters, and *C. leucas* is especially  
463 known as a tropical to sub-tropical species (Simpfendorfer and Burgess, 2009); in turn, *C.*  
464 *brachyurus* is a more temperate species that thrives in relatively cooler waters (Duffy & Gordon,  
465 2003). Another carcharhinid genus, *Galeocerdo*, is known from the P0 by several teeth of the  
466 extinct species *Galeocerdo aduncus*, whose closest living relative (i.e., the tiger shark *Galeocerdo*  
467 *cuvier*) is known as a tropical/subtropical fish (Ferreira and Simpfendorfer, 2019); similar  
468 considerations also apply to the sole extant species of *Anoxypristis* (i.e., the knifetooth sawfish



469 *Anoxypristis cuspidata*; D'Anastasi et al., 2013), a genus of rays that is represented in the lower  
470 Pisco strata by several rostral spines that could not be determined at the species level. A  
471 predilection for tropical and warm-temperate waters is also regarded as characteristic of the extinct  
472 sharks *Carcharocles megalodon* (Purdy, 1996; Aguilera and Aguilera, 2004; but see also Pimiento  
473 et al., 2013, for a different interpretation) and *Hemipristis serra*; in particular, the extant  
474 snaggletooth shark *Hemipristis elongata* – the only living species of *Hemipristis* – is a tropical  
475 coastal shark that inhabits inshore and offshore waters up to 30 m depth (Compagno, 1984;  
476 Pimiento et al., 2013).

477

## 478 **5. Discussion**

### 479 *5.1. SIS age of the P0 strata*

480 Strontium data confirm a Burdigalian age for the Ct1 sequence of the Chilcatay Formation, in  
481 line with the  $^{39}\text{Ar}$ – $^{40}\text{Ar}$  dating on tephra and with the biostratigraphic results given by diatoms and  
482 silicoflagellates from the localities of Roca Negra and Ullujaya (Belia and Nick, 2016; Di Celma et  
483 al., 2018b; Bosio et al., in press). This SIS ages are in agreement with the older age of  $19.25 \pm 0.05$   
484 Ma of the PN-T2 ash layer dated by Bosio et al. (in press) at the base of the Chilcatay Formation at  
485 Roca Negra, and with the ages of  $19.00 \pm 0.28$  Ma and  $18.02 \pm 0.07$  Ma obtained from ash layers at  
486 the base and at the top of the Ullujaya succession (UJA-T35 and SOT-T3, respectively, of Bosio et  
487 al., in press; Di Celma et al., 2018b). In addition, they are consistent in themselves, with  
488 stratigraphically lower beds yielding older or at least matching ages, although this observation is  
489 limited by the broadly overlapping error ranges for each layer. Overall, the consistency of the  
490 strontium dates from the Ct1 sequence confirms the suitability of the method for dating sediments  
491 in the East Pisco Basin.

492 Our results also provide the first direct evidence for the age of the P0 sequence of the Pisco  
493 Formation in the study area, placing this unit in the middle Miocene (Langhian–Serravallian). This  
494 estimate is again consistent with the broad age constraints (ca. 9.5–18.0 Ma) imposed by previous  
495 radiometric dating and biostratigraphy (Di Celma et al., 2018b; Bosio et al., in press).

496 Current knowledge about both invertebrate and vertebrate assemblages of the P0 sequence is  
497 poorly informative in terms of chronostratigraphy; that said, a middle Miocene age matches the  
498 general aspect of the P0 oryctocoenosis. Indeed, mollusks suggest similarities with the lower–  
499 middle Miocene Navidad Formation of central Chile (DeVries and Frassinetti, 2003). Likewise, the  
500 baleen whale assemblage appears remarkably more archaic than that of the overlying P1 and P2  
501 sequences (Di Celma et al., 2017; Marx et al., 2017b), with the presence of *Pelocetus* sp. (Bianucci  
502 et al., 2019) matching other early–middle Miocene occurrences of this genus from Japan (Kimura et

503 al., 2007) and eastern North America (Kellogg, 1965). The occurrence of the archaic cetotheriid  
504 *Tiucetus rosae*, the earliest branching member of a mysticete family (i.e., Cetotheriidae) that  
505 flourished in late Miocene times (Marx et al., 2019b), also characterizes the P0 oryctocoenosis,  
506 possibly hinting at a middle Miocene age. Also notable is the abrupt increase in baleen whale  
507 abundance relative to the underlying Chilcatay Formation, which appears to reflect a global early–  
508 middle Miocene pattern (Bianucci et al., 2018b; Marx et al., 2019a). Sharks and rays are of limited  
509 utility, as all the taxa recognized so far exhibit a stratigraphic range which spans for most of the  
510 Miocene at least. As a consequence, all the elasmobranch taxa recognized from the P0 sequence but  
511 *Carcharocles megalodon* and *Hemipristis serra*, are known from both the lower Miocene Chilcatay  
512 strata exposed in the Ullujaya-Zamaca areas (Bianucci et al., 2018b; Di Celma et al., 2018b, 2019;  
513 Landini et al., 2019) and the upper Miocene Pisco strata (P1 and P2 sequences) exposed at Cerro  
514 Colorado (Di Celma et al., 2017; Landini et al., 2017a, b). *Carcharocles megalodon*, whose fossil  
515 record starts with the Burdigalian (Carrillo-Briceño et al., 2019, but see also Perez et al., 2019, at  
516 this regard), is well-known from the P1 and P2 beds but absent from the Chilcatay Formation,  
517 where the genus *Carcharocles* is represented by the more archaic species *C. chubutensis*.  
518 Conversely, *Hemipristis serra* is present in the Burdigalian deposits of the Chilcatay Formation,  
519 whereas it is absent from the younger P1 and P2 sequences, although it is known from outside the  
520 East Pisco Basin in deposits as young as the early Pleistocene (Ebersole et al., 2017).

521

## 522 5.2. Paleoclimatic significance of the P0 fossil assemblage

523 Previous investigations on the invertebrate assemblages from the P0 and P1 sequences revealed a  
524 marked faunal change coincident with the PE0.1 unconformity (Di Celma et al., 2017) (Fig. 3D).  
525 Specifically, species such as *Ficus distans* and *Miltha cf. vidali*, which also occur in the Chilcatay  
526 Formation, associate P0 with the Navidad Formation of Chile, rather than the Panamic fauna  
527 (DeVries, 2002, 2007; DeVries and Frassinetti, 2003). According to Nielsen and Glodny (2009), an  
528 interpretation of the mollusk assemblage from the Navidad Formation in the light of the ecological  
529 preference of extant genera suggests water temperatures of at least 20°C for the Navidad area  
530 (34°S) during the early-middle Miocene. Indeed, the presence in the P0 sequence of warm-water or  
531 tropical taxa such as Architectonicidae and Cypraeidae (DeVries and Frassinetti, 2003; Nielsen and  
532 Frassinetti, 2007) (see Fig. 8A–C, H–J), as well as the occurrence of *Ficus*, indicates a warm-water,  
533 tropical paleoenvironment for this unit. This is also supported by the finding of the only coral  
534 colony ever collected from the East Pisco Basin, belonging to the family Rhizangiidae (Fig. 8F, G).  
535 Rhizangiid scleractinians are the most common corals in shallow-water tropical and warm  
536 temperate environments of the eastern Pacific; in particular, the P0 specimens appear as

537 morphologically close to the Miocene to Holocene genus *Culicia*, which currently lives in the  
538 tropical waters of the Indo-Pacific region (Cairns et al., 2005). On the whole, these observations  
539 support the paleoclimatic reconstruction proposed by DeVries and Frassinetti (2003), who  
540 hypothesized warm-water conditions for the southern Peruvian coast during the early and middle  
541 Miocene, in contrast with the cooler conditions during the late Miocene and early Pliocene.

542 Our data on the composition of the vertebrate oryctocoenosis from P0 also indicate tropical to  
543 subtropical thermal affinities for the paleoenvironment. In particular, among the recognized taxa,  
544 the knifetooth sawfish *Anoxypristis* is currently known as a nectobenthic organism that inhabits  
545 coastal and estuarine warm-water environments (e.g., D’Anastasi, 2013). Similarly, the extinct  
546 snaggletooth shark *Hemipristis serra* (Fig. 8D, E) is one of the most common chondrichthyan taxa  
547 in low-latitude neritic deposits of the Neogene, and its closest extant relative (*Hemipristis elongata*)  
548 is known as a tropical nearshore shark that inhabits coastal waters not deeper than about 30 m (e.g.,  
549 Compagno, 1984). Interestingly, there are no late Miocene occurrences of *H. serra* from the East  
550 Pisco Basin, even though this species persisted till the early Pleistocene in many tropical/subtropical  
551 chondrichthyan assemblages worldwide, and has even been recorded from the late Miocene strata of  
552 the Miramar Formation of northern Peru (Apolín et al., 2004).

553 It should be noted that the deposition of the P0 strata likely took place during the last phases of  
554 the Middle Miocene Climatic Optimum (= MMCO, the last major warming interval of the  
555 Cenozoic, occurred between 17 and 14 Ma; Loughney et al., 2019, and references therein) or the  
556 onset of the Middle Miocene Climatic Transition (= MMCT, the subsequent interval of gradual  
557 change towards cooler climatic conditions), i.e., during a period of globally high temperatures  
558 relative to the modern. As reported above, the warm, tropical paleoenvironment here reconstructed  
559 for the P0 sequence sets it apart from the remainder of the Pisco Formation, which is thought to  
560 reflect a cooler setting (e.g., Dunbar et al., 1990; DeVries and Frassinetti, 2003; Amiot et al., 2008;  
561 Di Celma et al., 2017). In particular, oxygen-isotope analyses on phosphatic remains of marine  
562 vertebrates from upper Miocene horizons of the Pisco Formation exposed in the Ica desert (i.e., the  
563 CLB vertebrate level of Muizon and DeVries, 1985; referred to the late Miocene according to Di  
564 Celma et al., 2017) and the Sacaco area (i.e., the ELJ, AGL, SAS and SAO vertebrate levels of  
565 Muizon and DeVries, 1985; late Miocene in age according to Ehret et al., 2012) have revealed  
566 marine paleotemperatures that, on the whole, match those observed today off the coasts of Peru  
567 (Amiot et al., 2008). Overall, this pattern is suggestive of relatively cool conditions along the  
568 Peruvian coast during the late Miocene, which could be regarded as reflecting the post-MMCO  
569 trend of global cooling that culminated with ocean temperatures dipping to near-modern values  
570 around 7 and 5.4 Ma (Herbert et al., 2016). Furthermore, since the upper Miocene deposits of the

571 Pisco Formation contain abundant diatomaceous siltstones that indicate the existence of high  
572 primary productivity resulting from strong and persistent coastal upwelling conditions (Dunbar et  
573 al., 1990; DeVries and Frassinetti, 2003; Di Celma et al., 2017), it is reasonable to hypothesize that  
574 the above pattern is also representative of a major regional oceanographic change – i.e., a middle or  
575 early late Miocene strengthening of the Humboldt Current (see also conclusion in Amiot et al.,  
576 2008). This change might also explain the local disappearance of *H. serra*, whose range likely  
577 contracted northwards as colder conditions took hold along the coasts of southern Peru.

578

## 579 **6. Conclusions**

580 Along the western side of the Ica River (Peru), the age of deposition of the P0 sequence, the lowest  
581 stratigraphic unit of the Pisco Formation, was an uncertain and debated issue. In the present study,  
582 Strontium Isotope Stratigraphy was applied on carbonates and phosphates of both the Chilcatay and  
583 Pisco formations for resolving the age of this paleontologically significant unit.

584 In this work, we provide new Burdigalian ages (18.8–18.0 Ma) for the Ct1 sequence of the  
585 Chilcatay Formation and propose a Langhian–Serravallian age (14.8–12.4 Ma) for the P0 sequence  
586 of the Pisco Formation (see Fig. 9). This estimate is consistent with the relatively archaic aspect of  
587 the fossil assemblage from the lower Pisco strata, and provides a time constraint for a marked  
588 faunal change occurring across the PE0.1 unconformity. With respect to the Chilcatay Formation,  
589 the obtained Sr ages perfectly agree with previous  $^{39}\text{Ar}$ – $^{40}\text{Ar}$  ages on tephra layers and  
590 biostratigraphic results, confirming the feasibility of SIS in the studied deposits. This gives further  
591 reliability to the middle Miocene ages obtained by means of Sr isotope analyses for the P0  
592 sequence.

593 Not least, both the invertebrate and vertebrate fossil assemblages indicate that the P0 sequence  
594 was deposited in a warm-water environment resembling that of the underlying Chilcatay Formation,  
595 but contrasting with the cooler and more productive setting of the overlying P1 and P2 sequences.  
596 We suggest that the marked cooling distinguishing P0 from the remainder of the Pisco Formation  
597 may reflect both the late Miocene trend of global cooling and a middle–late Miocene strengthening  
598 of the Humboldt Current.

599

## 600 **Acknowledgments**

601 The authors are grateful to T.J. DeVries for information and helpful discussions on the age and  
602 paleoenvironment of the Pisco Formation. Special thanks to W. Landini, O. Lambert and C. de  
603 Muizon for interesting discussions on the vertebrate fauna, and to D. Basso and G. Coletti for  
604 helpful discussions on mollusk systematics and strontium dating. The authors would like to thank

605 also R. Varas-Malca and W. Aguirre for assistance in the field, and D. Buhl for running the ICP-  
606 OES and Sr isotope analyses at Bochum University. The authors wish to thank the journal  
607 reviewers F. Núñez for his valuable contribution and J. McArthur for the helpful criticism and for  
608 sharing the LOWESS 5 Table.

609

## 610 **Funding**

611 This study was supported by grants from the Italian Ministero dell'Istruzione dell'Università e  
612 della Ricerca (PRIN Project 2012YJSBMK) to G.Bi.; from the Università degli Studi di Milano-  
613 Bicocca to E.M. (2017-ATE-0466); from the Università di Pisa to G.Bi. (PRA\_2017\_0032); and an  
614 EU Marie Skłodowska-Curie Global Postdoctoral fellowship (656010/ MYSTICETI) and an  
615 Australian Research Council DECRA fellowship (DE190101052) to F.G.M.

616

## 617 **Bibliography**

618 Aguilera, O.A., Aguilera, D.R. (2004). Giant-toothed white sharks and wide-toothed mako  
619 (Lamnidae) from the Venezuela Neogene: their role in the Caribbean, shallow-water fish  
620 assemblage. *Caribbean Journal of Science*, 40, 368-382.

621 Amiot, R., Göhlich, U. B., Lécuyer, C., Muizon, C. de, Cappetta, H., Fourel, F., Hérin, M.-A.,  
622 Martineau, F. (2008). Oxygen isotope compositions of phosphate from Middle Miocene–Early  
623 Pliocene marine vertebrates of Peru. *Palaeogeography, Palaeoclimatology, Palaeoecology*, 264,  
624 85-92.

625 Apolín, J., González, G., Martínez, J.M. (2004). Seláceos del Mioceno Superior de Quebrada  
626 Pajaritos (Piura, Perú). *Actas XII Congreso Peruano de Geología, Sociedad Geológica del Perú,*  
627 *Perú*, 401-404.

628 Barbin, V., Ramseyer, K., Debenay, J.P., Schein, E., Roux, M., Decrouez, D. (1991).  
629 Cathodoluminescence of recent biogenic carbonates: an environmental and ontogenetic  
630 fingerprint. *Geological Magazine*, 128, 19-26.

631 Barbin, V. (2013). Application of cathodoluminescence microscopy to recent and past biological  
632 materials: a decade of progress. *Mineralogy and Petrology*, 107, 353-362.

633 Becker, A.M., Seidemann, D.E., Chamberlain, J.A. Jr., Buhl, D., Slattery, W. (2008). Strontium  
634 isotopic signatures in the enameloid and dentine of upper Cretaceous shark teeth from western  
635 Alabama: Paleoecologic and geochronologic implications. *Palaeogeography, Palaeoclimatology,*  
636 *Palaeoecology*, 264, 188-194.

637 Belia, E.R., Nick, K.E. (2016). Early-Miocene calcareous nannofossil biostratigraphy from low-  
638 latitude, Pisco Basin, Peru. *Geological Society of America Abstracts with Programs*, 48, 4.

- 639 Belia, E.R., Nick, K.E., Bedoya Agudelo, E., Watkins, D.K. (2019). Earliest Miocene calcareous  
640 nannofossil biostratigraphy from the low-latitude Pisco Basin (Peru). *Stratigraphy*, 16, 87-105.
- 641 Bianucci, G., Collareta, A., Bosio, G., Landini, W., Gariboldi, K., Gioncada, A., Lambert, O.,  
642 Malinverno, E., de Muizon, C., Varas-Malca, R., Villa, I.M, Coletti, G., Urbina, M., Di Celma,  
643 C. (2018b). Taphonomy and palaeoecology of the lower Miocene marine vertebrate assemblage  
644 of Ullujaya (Chilcatay Formation, East Pisco Basin, southern Peru). *Palaeogeography,*  
645 *Palaeoclimatology, Palaeoecology*, 511, 256-279.
- 646 Bianucci, G., Di Celma, C., Collareta, A., Landini, W., Post, K., Tinelli, C., de Muizon, C., Bosio,  
647 G., Gariboldi, K., Gioncada, A., Malinverno, E., Cantalamessa G., Altamirano-Sierra, A, Salas-  
648 Gismondi, R., Urbina, M., Lambert, O. (2016a). Fossil marine vertebrates of Cerro Los Quesos:  
649 Distribution of cetaceans, seals, crocodiles, seabirds, sharks, and bony fish in a late Miocene  
650 locality of the Pisco Basin, Peru. *Journal of Maps*, 12, 1037-1046.
- 651 Bianucci, G., Di Celma, C., Landini, W., Post, K., Tinelli, C., de Muizon, C., Gariboldi, K.,  
652 Malinverno, E., Cantalamessa, G., Gioncada, A., Collareta, A., Salas-Gismondi, R., Varas-  
653 Malca, R.M., Urbina, M., Lambert, O. (2016b). Distribution of fossil marine vertebrates in Cerro  
654 Colorado, the type locality of the giant raptorial sperm whale *Livyatan melvillei* (Miocene, Pisco  
655 Formation, Peru). *Journal of Maps*, 12, 543-557.
- 656 Bianucci, G., Urbina, M., Lambert, O. (2015). A new record of *Notocetus vanbenedeni*  
657 (*Squalodelphinidae*, *Odontoceti*, *Cetacea*) from the early Miocene of Peru. *Comptes Rendus*  
658 *Palevol*, 14, 5-13.
- 659 Bianucci, G., Bosio, G., Malinverno, E., de Muizon, C., Villa, I. M., Urbina, M., Lambert, O.  
660 (2018a). A new large squalodelphinid (*Cetacea*, *Odontoceti*) from Peru sheds light on the Early  
661 Miocene platanistoid disparity and ecology. *Royal Society Open Science*, 5, 172302.
- 662 Bianucci, G., Marx, F.G., Collareta, A., Di Stefano, A., Landini, W., Morigi, C., Varola, A. (2019).  
663 Rise of the titans: baleen whales became giants earlier than thought. *Biology Letters*, 15,  
664 20190175.
- 665 Bosio, G., Gioncada, A., Malinverno, E., Di Celma, C., Villa, I. M., Cataldi, G., Gariboldi, K.,  
666 Collareta, A., Urbina, M., Bianucci, G. (2019). Chemical and petrographic fingerprinting of  
667 volcanic ashes as a tool for high-resolution stratigraphy of the upper Miocene Pisco Formation  
668 (Peru). *Journal of the Geological Society*, 176, 13-28.
- 669 Bosio, G., Malinverno, E., Villa, I.M., Di Celma, C., Gariboldi, K., Gioncada, A., Barberini, B.,  
670 Urbina, M., Bianucci, G. (in press). Tephrochronology and chronostratigraphy of the Miocene  
671 Chilcatay and Pisco formations (East Pisco Basin, Peru). *Newsletter on Stratigraphy*, DOI:  
672 10.1127/nos/2019/0525.



- 673 Brand, L.R., Esperante, R., Chadwick, A.V., Porras, O. P., Alomía, M. (2004). Fossil whale  
674 preservation implies high diatom accumulation rate in the Miocene–Pliocene Pisco Formation of  
675 Peru. *Geology*, 32, 165-168.
- 676 Brand, U. (1991). Strontium Isotope Diagenesis of Biogenic Aragonite and Low-Mg Calcite.  
677 *Geochimica et Cosmochimica Acta*, 55, 505-513.
- 678 Brand, U., Jiang, G., Azmy, K., Bishop, J., Montanez, I.P. (2012). Diagenetic evaluation of a  
679 Pennsylvanian carbonate succession (Bird Spring Formation, Arrow Canyon, Nevada, U.S.A.)  
680 — 1: Brachiopod and whole rock comparison. *Chemical Geology*, 308/309, 26-39.
- 681 Brand, U., Veizer, J. (1980). Chemical Diagenesis of a Multicomponent Carbonate System -1:  
682 Trace Elements. *Journal of Sedimentary Research*, 50, 1219-1236.
- 683 Cairns, S.D., Häussermann, V., Försterra, G. (2005) A review of the Scleractinia (Cnidaria:  
684 Anthozoa) of Chile, with the description of two new species. *Zootaxa*, 1018, 15-46.
- 685 Carrillo-Briceño, J.D., Maxwell, E., Aguilera, O.A., Sánchez, R., Sánchez-Villagra, M.R. (2015).  
686 Sawfishes and other elasmobranch assemblages from the Mio-Pliocene of the South Caribbean  
687 (Urumaco Sequence, Northwestern Venezuela). *PLOS ONE*, 10, article #e0139230.
- 688 Coletti, G., Bosio, G., Collareta, A., Buckeridge, J., Consani, S., El Kateb, A. (2018).  
689 Palaeoenvironmental analysis of the Miocene barnacle facies: case studies from Europe and  
690 South America. *Geologica Carpathica*, 69, 573-592.
- 691 Coletti, G., Collareta, A., Bosio, G., Buckeridge, J., Urbina M. (in press). *Perumegabalanus calziai*  
692 gen. et sp. nov., a new intertidal megabalanine barnacle from the early Miocene of Peru. *Neues*  
693 *Jahrbuch für Geologie und Paläontologie-Abhandlungen*.
- 694 Collareta, A., Coletti, G., Bosio, G., Buckeridge, J., de Muizon, C., DeVries, T.J., Varas-Malca, R.,  
695 Altamirano-Sierra, A., Urbina-Schmitt, M., Bianucci, G. (2019). A new barnacle (Cirripedia:  
696 Neobalanoformes) from the early Miocene of Peru: Palaeoecological and palaeobiogeographical  
697 implications. *Neues Jahrbuch für Geologie und Paläontologie-Abhandlungen*, 292, 321-338.
- 698 Collareta, A., Landini, W., Chalcatana, C., Valdivia, W., Altamirano-Sierra, A., Urbina-Schmitt,  
699 M., Bianucci, G. (2017). A well preserved skeleton of the fossil shark *Cosmopolitodus hastalis*  
700 from the late Miocene of Peru, featuring fish remains as fossilized stomach contents. *Rivista*  
701 *Italiana di Paleontologia e Stratigrafia*, 123, 11-22.
- 702 Collareta, A., Landini, W., Lambert, O., Post, K., Tinelli, C., Di Celma, C., Panetta, D., Tripodi,  
703 M., Salvadori, P.A., Caramella, D., Marchi, D., Urbina, M., Bianucci, G. (2015). Piscivory in a  
704 Miocene Cetotheriidae: first record of fossilized stomach content for an extinct baleen-bearing  
705 whale. *The Science of Nature*, 102, article #70.

- 706 Compagno, L.J.V. (1984). FAO Species Catalogue. Vol 4: Sharks of the world, Part 2 -  
707 Carcharhiniformes. FAO Fisheries Synopsis No. 125, 4 (2), 251-633.
- 708 Cox, L.R., Newell, N.D., Boyd, D.W., Branson, C.C., Casey, R., Chavan, A., Coogan, A.H.,  
709 Dechaseaux, C., Fleming, C.A., Haas, F., Hertlein, L.G., Kauffman, E.G., Keen A.M., Larocque,  
710 A., McAlester, A.L., Moore, R.C., Nuttall, C.P., Perkins, B.F., Purl, H.S., Smith, L.A., Soot-  
711 Ryen, T., Stenzel, H.B., Trueman, E.R., Turner, R.T., Weir J. (1971). Part N. Mollusca  
712 (Bivalvia). In: Moore, R.C. (Ed.), Treatise of Invertebrate Paleontology. Lawrence, Meriden and  
713 New York, The University of Kansas Printing Service, N1-N1224.
- 714 Crippa, G., Ye, F., Malinverno, C., Rizzi, A. (2016). Which is the best method to prepare  
715 invertebrate shells for SEM analysis? Testing different techniques on recent and fossil  
716 brachiopods. Bollettino della Società Paleontologica Italiana, 55, 111-125.
- 717 D'Anastasi, B., Simpfendorfer, C., van Herwerden, L. (2013). *Anoxypristis cuspidata*. In: The  
718 IUCN Red List of Threatened Species 2013: e.T39389A18620409. <http://www.iucnredlist.org>,  
719 accessed on April 28, 2018.
- 720 DeVries, T.J. (2002). Patterns of diversity in Cenozoic marine mollusks from the Peruvian  
721 province. Geological Society of America Abstracts with Programs, 34, 39.
- 722 DeVries, T.J. (2007). Molluscan evidence bearing on Cenozoic warm upwelling off southern Peru.  
723 Geological Society of America Abstracts with Programs, 39, 78.
- 724 DeVries, T.J., Jud, N.A. (2018). Lithofacies patterns and paleogeography of the Miocene Chilcatay  
725 and lower Pisco depositional sequences (East Pisco Basin, Peru). Boletín de la Sociedad  
726 Geológica del Perú, Volumen Jubilar, 8, 124-167.
- 727 DeVries, T.J. (1998). Oligocene deposition and Cenozoic sequence boundaries in the Pisco Basin  
728 (Peru). Journal of South American Earth Sciences, 11, 217-231.
- 729 DeVries, T.J. (2016). Fossil Cenozoic crassatelline bivalves from Peru: New species and generic  
730 insights. Acta Palaeontologica Polonica, 61, 661-688.
- 731 DeVries, T.J., Frassinetti, D. (2003). Range extensions and biogeographic implications of Chilean  
732 Neogene mollusks found in Peru. Boletín del Museo Nacional de Historia Natural, Chile, 52,  
733 119-135.
- 734 DeVries, T.J., Groves, L.T., Urbina, M. (2006). A new early miocene Muracypraea Woodring, 1957  
735 (Gastropoda: Cypraeidae) from the Pisco Basin of southern Peru. The Nautilus, 120, 101-105.
- 736 DeVries, T.J., Schrader, H. (1997). Middle Miocene marine sediments in the Pisco Basin (Peru).  
737 Boletín de la Sociedad Geológica del Perú, 87, 1-13.
- 738 Di Celma, C., Malinverno, E., Bosio, G., Collareta, A., Gariboldi, K., Gioncada, A., Molli, G.,  
739 Basso, D., Varas-Malca, R.M., Pierantoni, P.P., Villa, I.M., Lambert, O., Landini, W., Sarti, G.,

- 740 Cantalamessa, G., Urbina, M., Bianucci, G. (2017). Sequence stratigraphy and paleontology of  
741 the upper Miocene Pisco Formation along the western side of the lower Ica valley (Ica Desert,  
742 Peru). *Rivista Italiana Paleontologia e Stratigrafia*, 123, 255-274.
- 743 Di Celma, C., Malinverno, E., Bosio, G., Gariboldi, K., Collareta, A., Gioncada, A., Landini, W.,  
744 Pierantoni, P.P., Bianucci, G. (2018a). Intraformational unconformities as a record of late  
745 Miocene eustatic falls of sea level in the Pisco Formation (southern Peru). *Journal of Maps*, 14,  
746 607-619.
- 747 Di Celma, C., Malinverno, E., Collareta, A., Bosio, G., Gariboldi, K., Lambert, O., Landini, W.,  
748 Gioncada, A., Villa, I.M., Coletti, G., de Muizon, C., Urbina, M., Bianucci, G. (2018b). Facies  
749 analysis, stratigraphy and marine vertebrate assemblage of the early Miocene Chilcatay  
750 Formation at Ullujaya (Pisco basin, Peru). *Journal of Maps*, 14, 257-268.
- 751 Di Celma, C., Pierantoni, P.P., Malinverno, E., Collareta, A., Lambert, O., Landini, W., Bosio, G.,  
752 Gariboldi, K., Gioncada, A., de Muizon, C., Molli, G., Marx, F.G., Varas-Malca, R.M., Urbina,  
753 M., Bianucci, G. (2019). Allostratigraphy and paleontology of the lower Miocene Chilcatay  
754 Formation in the Zamaca area, East Pisco basin, southern Peru. *Journal of Maps*, 15, 393-405.
- 755 Duffy, C., Gordon, I. (2003). *Carcharhinus brachyurus*. In: The IUCN Red List of Threatened  
756 Species 2003: e.T41741A10551730. <http://www.iucnredlist.org>, accessed on April 28, 2018.
- 757 Dunbar, R.B., Marty, R.C., Baker, P.A. (1990). Cenozoic marine sedimentation in the Sechura and  
758 Pisco basins, Peru. *Palaeogeography, Palaeoclimatology, Palaeoecology*, 77, 235-261.
- 759 Ebersole, J.A., Ebersole, S.M., Cicimurri, D.J. (2017). The occurrence of early Pleistocene marine  
760 fish remains from the Gulf Coast of Mobile County, Alabama, USA. *Palaeodiversity*, 10, 97-116.
- 761 Ehret, D.J., MacDaffen, B.J., Jones, D.S., DeVries, T.J., Foster, D.A., Salas-Gismondi, R. (2012).  
762 Origin of the white shark *Carcharodon* (Lamniformes: Lamnidae) based on recalibration of the  
763 upper Neogene Pisco Formation of Peru. *Palaeontology*, 55, 1139-1153.
- 764 Enax, J., Janus, A. M., Raabe, D., Epple, M., Fabritius, H. O. (2014). Ultrastructural organization  
765 and micromechanical properties of shark tooth enameloid. *Acta Biomaterialia*, 10, 3959-3968.
- 766 Esperante, R., Brand, L., Nick, K. E., Poma, O., Urbina, M. (2008). Exceptional occurrence of  
767 fossil baleen in shallow marine sediments of the Neogene Pisco Formation, Southern Peru.  
768 *Palaeogeography, Palaeoclimatology, Palaeoecology*, 257, 344-360.
- 769 Faure, G., Mensing, T.M. (2005). *Isotopes: Principles and Applications*. New York, John Wiley &  
770 Sons.
- 771 Ferreira, L. C., Simpfendorfer, C. (2019). *Galeocerdo cuvier*. In: The IUCN Red List of Threatened  
772 Species 2019:e.T39378A291354. <http://www.iucnredlist.org>, accessed on March 25, 2019.
- 773 Föllmi, K.B. (2016). Sedimentary condensation. *Earth-Science Reviews*, 152, 143-180.

- 774 Frijia, G., Parente, M. (2008). Strontium isotope stratigraphy in the upper Cenomanian shallow-  
775 water carbonates of the southern Apennines: Short-term perturbations of marine  $^{87}\text{Sr}/^{86}\text{Sr}$  during  
776 the oceanic anoxic event 2. *Palaeogeography, Palaeoclimatology, Palaeoecology*, 261, 15-29.
- 777 Frijia, G., Parente, M., Di Lucia, M., Mutti, M. (2015). Carbon and strontium isotope stratigraphy  
778 of the Upper Cretaceous (Cenomanian-Campanian) shallow-water carbonates of southern Italy:  
779 Chronostratigraphic calibration of larger foraminifera biostratigraphy. *Cretaceous Research*, 53,  
780 110-139.
- 781 Gariboldi, K., Bosio, G., Malinverno, E., Gioncada, A., Di Celma, C., Villa, I.M., Urbina, M.,  
782 Bianucci, G. (2017). Biostratigraphy, geochronology and sedimentation rates of the upper  
783 Miocene Pisco Formation at two important marine vertebrate fossil-bearing sites of southern  
784 Peru. *Newsletters on Stratigraphy*, 50, 417-444.
- 785 Gariboldi, K., Gioncada, A., Bosio, G., Malinverno, E., Di Celma, C., Tinelli, C., Cantalamessa, G.,  
786 Landini, W., Urbina, M., Bianucci, G. (2015). The dolomite nodules enclosing fossil marine  
787 vertebrates in the East Pisco Basin, Peru: field and petrographic insights into the Lagerstätte  
788 formation. *Palaeogeography, Palaeoclimatology, Palaeoecology*, 438, 81-95.
- 789 Gioncada, A., Collareta, A., Gariboldi, K., Lambert, O., Di Celma, C., Bonaccorsi, E., Urbina, M.,  
790 Bianucci, G. (2016). Inside baleen: exceptional microstructure preservation in a late Miocene  
791 whale skeleton from Peru. *Geology*, 44, 839-842.
- 792 Gioncada, A., Gariboldi, K., Collareta, A., Di Celma, C., Bosio, G., Malinverno, E., Lambert, O.,  
793 Pike, J., Urbina, M., Bianucci, G. (2018a). Looking for the key to preservation of fossil marine  
794 vertebrates in the Pisco Formation of Peru: new insights from a small dolphin skeleton. *Andean  
795 Geology*, 45, 379-398.
- 796 Gioncada, A., Petrini, R., Bosio, G., Gariboldi, K., Collareta, A., Malinverno, E., Bonaccorsi, E., Di  
797 Celma, C., Pasero, M., Urbina, M., Bianucci, G. (2018b). Insights into the diagenetic  
798 environment of fossil marine vertebrates of the Pisco Formation (late Miocene, Peru) from  
799 mineralogical and Sr-isotope data. *Journal of South American Earth Sciences*, 81, 141-152.
- 800 Hampel, A., Kukowski, N., Bialas, J., Heubscher, C., Heinbockel, R. (2004). Ridge subduction at  
801 an erosive margin: the collision zone of the Nazca Ridge in southern Peru. *Journal of  
802 Geophysical Research*, 109, article #B02101.
- 803 Harrel, T.L. Jr, Pérez-Huerta, A., Phillips, G. (2016). Strontium isotope age-dating of fossil shark  
804 tooth enameloid from the Upper Cretaceous Strata of Alabama and Mississippi, USA. *Cretaceous  
805 Research*, 62, 1-12.

- 806 Herbert, T. D., Lawrence, K. T., Tzanova, A., Peterson, L. C., Caballero-Gill, R., Kelly, C. S.  
807 (2016). Late Miocene global cooling and the rise of modern ecosystems. *Nature Geoscience*, 9,  
808 843.
- 809 Hsu, J.T., 1992. Quaternary uplift of the Peruvian coast related to the subduction of the Nazca  
810 Ridge: 13.5 to 15.6 degrees South latitude. *Quaternary International*, 15/16, 87-97.
- 811 Kellogg, R. (1965). Fossil marine mammals from the Miocene Calvert Formation of Maryland and  
812 Virginia, part 1: a new whalebone whale from the Miocene Calvert Formation. *United States*  
813 *National Museum Bulletin*, 247, 1-45.
- 814 Kimura, T., Hasegawa, Y., Ohzawa, H., Yamaoka, T., Furukawa, Y., Ueda, T., Kiyoshi, T.,  
815 Sugihara, M., Sakuda, M. (2007). A mysticete whale (Cetacea) skeleton from the middle  
816 Miocene Bihoku Group, Shobara, Hiroshima, Japan. *Miscellaneous Reports of the Hiwa*  
817 *Museum for Natural History*, 48, 1-10.
- 818 Kulm, L.D., Resig, J.M., Thornburg, T.M., Schrader, H.J. (1982). Cenozoic structure, stratigraphy  
819 and tectonics of the central Peru forearc. In: Legget, J.K. (Ed.), *Trench and forearc geology:*  
820 *sedimentation and tectonics on modern and ancient plate margins*. London, Blackwells, 151-169.
- 821 Lambert, O., Bianucci, G., de Muizon, C. (2017a). Macroraptorial sperm whales (Cetacea,  
822 Odontoceti, Physeteroidea) from the Miocene of Peru. *Zoological Journal of the Linnean*  
823 *Society*, 179, 404-474.
- 824 Lambert, O., Bianucci, G., Urbina, M. (2014). *Huaridelphis raimondii*, a new early Miocene  
825 *Squalodelphinidae* (Cetacea, odontoceti) from the Chilcatay Formation, Peru. *Journal of*  
826 *Vertebrate Paleontology*, 34, 987-1004.
- 827 Lambert, O., Bianucci, G., Urbina, M., Geisler, J.H. (2017b). A new inioid (Cetacea, Odontoceti,  
828 *Delphinidae*) from the Miocene of Peru and the origin of modern dolphin and porpoise families.  
829 *Zoological Journal of the Linnean Society*, 179, 919-946.
- 830 Lambert, O., Collareta, A., Landini, W., Post, K., Ramassamy, B., Di Celma, C., Urbina, M,  
831 Bianucci, G. (2015a). No deep diving: evidence of predation on epipelagic fish for a stem beaked  
832 whale from the Late Miocene of Peru. *Proceedings of the Royal Society B: Biological Sciences*,  
833 282, article #20151530.
- 834 Lambert, O., de Muizon, C., Malinverno, E., Di Celma, C., Urbina, M., Bianucci, G. (2018). A new  
835 odontocete (toothed cetacean) from the Early Miocene of Peru expands the morphological  
836 disparity of extinct heterodont dolphins. *Journal of Systematic Palaeontology*, 16, 981-1016.
- 837 Lambert, O., de Muizon, C., Bianucci, G. (2015b). A new archaic homodont toothed cetacean  
838 (Mammalia, Cetacea, Odontoceti) from the early Miocene of Peru. *Geodiversitas*, 37, 79-108.

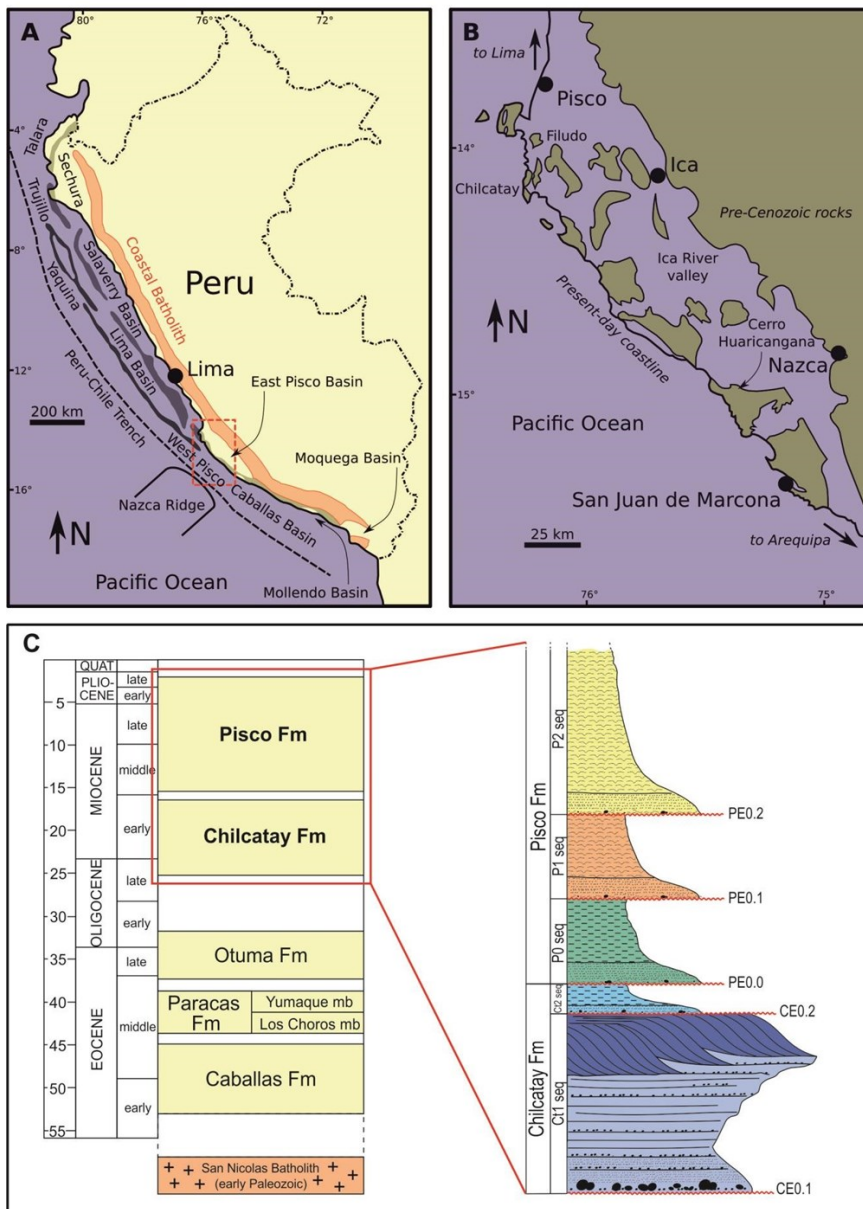
- 839 Landini, W., Altamirano-Sierra, A., Collareta, A., Di Celma, C., Urbina, M., Bianucci, G. (2017a).  
840 The late Miocene elasmobranch assemblage from Cerro Colorado (Pisco Formation, Peru).  
841 Journal of South American Earth Sciences, 73, 168-190.
- 842 Landini, W., Collareta, A., Pesci, F., Di Celma, C., Urbina, M., Bianucci, G. (2017b). A secondary  
843 nursery area for the copper shark *Carcharhinus brachyurus* from the late Miocene of Peru.  
844 Journal of South American Earth Sciences, 78, 164-174.
- 845 Landini, W., Collareta, A., Di Celma, C., Malinverno, E., Urbina, M., Bianucci, G. (2019) The early  
846 Miocene elasmobranch assemblage from Zamaca (Chilcatay Formation, Peru). Journal of South  
847 American Earth Sciences, 91, 352-371.
- 848 León, W., Aleman, A., Torres, V., Rosell, W., De la Cruz, O. (2008). Estratigrafía, sedimentología  
849 y evolución tectónica de la cuenca Pisco Oriental. Boletín INGEMMET, 27, 144 pp.
- 850 Loughney, K. M., Hren, M. T., Smith, S. Y., Pappas, J. L. (2019). Vegetation and habitat change in  
851 southern California through the Middle Miocene Climatic Optimum: Paleoenvironmental records  
852 from the Barstow Formation, Mojave Desert, USA. Geological Society of America Bulletin.
- 853 Macharé, J., Ortlieb, L. (1992). Plio-Quaternary vertical motions and the subduction of the Nazca  
854 Ridge, central coast of Peru. Tectonophysics, 205, 97-108.
- 855 Marocco, R., de Muizon, C., (1988). Le Bassin Pisco, bassin cénozoïque d'avant arc de la côte du  
856 Pérou central: analyse géodynamique de son remplissage. Géodynamique, 3, 3-19.
- 857 Marx, F.G., Collareta, A., Gioncada, A., Post, K., Lambert, O., Bonaccorsi, E., Urbina, M.,  
858 Bianucci, G. (2017a). How whales used to filter: exceptionally preserved baleen in a Miocene  
859 cetotheriid. Journal of Anatomy, 231, 212-220.
- 860 Marx, F.G., Fitzgerald, E.M., Fordyce, R. E. (2019a). Like phoenix from the ashes: How modern  
861 baleen whales arose from a fossil "dark age". Acta Palaeontologica Polonica, 64, 231-238.
- 862 Marx, F.G., Lambert, O., de Muizon, C. (2017b). A new Miocene baleen whale from Peru  
863 deciphers the dawn of cetotheriids. Royal Society Open Science, 4, article #170560.
- 864 Marx, F.G., Post, K., Bosselaers, M., Munsterman, D.K. (2019). A large Late Miocene cetotheriid  
865 (Cetacea, Mysticeti) from the Netherlands clarifies the status of Tranatocetidae. PeerJ, 7, article  
866 #e6426.
- 867 McArthur, J. (1994). Recent Trends in Strontium Isotope Stratigraphy. Terra Nova, 6, 331-358.
- 868 McArthur, J.M., Howarth, R.J., Shields, G.A. (2012). Strontium Isotope Stratigraphy. In: Gradstein,  
869 F.M., Ogg, J.G., Schmitz, M., Ogg, G. (Eds.), The Geologic Time Scale 2012. Oxford, Elsevier,  
870 127-144.
- 871 Muizon, C. de, DeVries, T.J. (1985). Geology and paleontology of late Cenozoic marine deposits in  
872 the Sacaco area (Peru). Geologische Rundschau, 74, 547-563.



- 873 Nielsen, S.N., Frassinetti, D. (2007). The Miocene Architectonicidae (Gastropoda) of Chile.  
874 Paläontologische Zeitschrift, 81/3, 291-303.
- 875 Nielsen, S.N., Glodny, J. (2009). Early Miocene subtropical water temperatures in the southeast  
876 Pacific. Palaeogeography, Palaeoclimatology, Palaeoecology, 280, 480-488.
- 877 North American Commission on Stratigraphic Nomenclature [NACSN] (2005). North American  
878 stratigraphic code. American Association of Petroleum Geologists Bulletin, 89, 1547-1591.
- 879 Penven, P., Echevin, V., Pasapera, J., Colas, F., Tam, J. (2005). Average circulation, seasonal cycle,  
880 and mesoscale dynamics of the Peru Current System: a modeling approach. Journal of  
881 Geophysical Research, 110, C10021.
- 882 Perez, V.J., Godfrey, S.J., Kent, B.W., Weems, R.E., Nance, J.R. (2018). The transition between  
883 *Carcharocles chubutensis* and *Carcharocles megalodon* (Otodontidae, Chondrichthyes): lateral  
884 cusplet loss through time. Journal of Vertebrate Paleontology, 38, article #e1546732.
- 885 Pilger R.H. (1981). Plate reconstructions, aseismic ridges, and low-angle subduction beneath the  
886 Andes. Geological Society of America Bulletin, 92, 448-456.
- 887 Pimiento, C., MacFadden, B.J., Clements, C.F., Varela, S., Jaramillo, C., Velez-Juarbe, J., Silliman,  
888 B.R. (2016). Geographical distribution patterns of *Carcharocles megalodon* over time reveal  
889 clues about extinction mechanisms. Journal of Biogeography, 43, 1645-1655.
- 890 Purdy, R.W. (1996). Paleoecology of fossil white sharks. In: Klimley, A.P., Ainley, D.G. (Eds.),  
891 Great white sharks: the biology of *Carcharodon carcharias*, 67-78. San Diego, Academic Press.
- 892 Santos, A., Mayoral, E., Muñiz, F. (2005). Bioerosion scars of acorn barnacles from the  
893 southwestern Iberian Peninsula, upper Neogene. Rivista Italiana di Paleontologia e Stratigrafia,  
894 111, 181-189.
- 895 Scasso, R.A., McArthur, J.M., del Río, C.J., Martínez, S., Thirlwall, M.F. (2001).  $^{87}\text{Sr}/^{86}\text{Sr}$  Late  
896 Miocene age of fossil molluscs in the "Enterriense" of the Valdés Peninsula (Chubut,  
897 Argentina). Journal of South American Earth Sciences, 14, 319-329.
- 898 Simpfendorfer, C.A., Burgess, G.H. (2009). *Carcharhinus leucas*. In: The IUCN Red List of  
899 Threatened Species 2013: e.T39372A10187195. <http://www.iucnredlist.org>, accessed on April  
900 28, 2018.
- 901 Steuber, T. (1999). Isotopic and chemical intra-shell variations in low-Mg calcite of rudist bivalves  
902 (Mollusca: Hippuritacea): disequilibrium fractionations and Late Cretaceous seasonality.  
903 International Journal Earth Sciences, 88, 551-570.
- 904 Steuber, T. (2003). Strontium isotope chemostratigraphy of rudist bivalves and cretaceous carbonate  
905 platforms. In: Gili, E., Negra, M.E.H., Skelton, P.W. (Eds.), North African Cretaceous Carbonate  
906 Platform Systems. NATO Science Series, IV. Earth and Environmental Sciences, 28, 229-238.

- 907 Thornburg, T.M., Kulm, L.D. (1981). Sedimentary basins of the Peru continental margin: structure,  
908 stratigraphy, and Cenozoic tectonics from 6°S to 16°S latitude. In: Kulm, L.D., Dymond, J.,  
909 Dasch, E.J., Hussong, D.M. (Eds.), Nazca plate: crustal formation and Andean convergence.  
910 Geological Society of America Memoir, 154, 393-422.
- 911 Travis, R. B., Gonzales, G., Pardo, A. (1974). Hydrocarbon Potential of Coastal Basins of Peru.  
912 AAPG Bulletin, 58, 1460-1460.
- 913 Ullmann, C.V., Korte, C. (2015). Diagenetic alteration in low-Mg calcite from microfossils: a  
914 review. Geological Quarterly, 59, 3-20.
- 915 Zúñiga-Rivero, F.J., Klein, G.D., Hay-Roe, H., Álvarez-Calderon, E. (2010). The hydrocarbon  
916 potential of Peru. Lima, BPZ Exploración & Producción S.R.L.
- 917
- 918

919 **Figure captions**



920

921 **Figure 1. A.** Map of the major Cenozoic sedimentary basins along the Peruvian coast. Major  
 922 structural highs are the Coastal Batholith, the Outer Shelf High and the Upper Slope Ridge.  
 923 Redrawn and modified from Travis et al. (1976) and Thornburg and Kulm (1981). **B.**  
 924 Paleoenvironmental reconstruction of the Peruvian coast during the Miocene. Islands are  
 925 hypothesized on the basis of the distribution of the pre-Cenozoic rocks. Redrawn and modified from  
 926 DeVries and Schrader (1997). **C.** Schematic stratigraphic column of the East Pisco Basin (from  
 927 Eocene to Recent, ages are in Ma) with a close-up of the Chilcatay and Pisco formations and their  
 928 internal subdivisions in sequences.

929

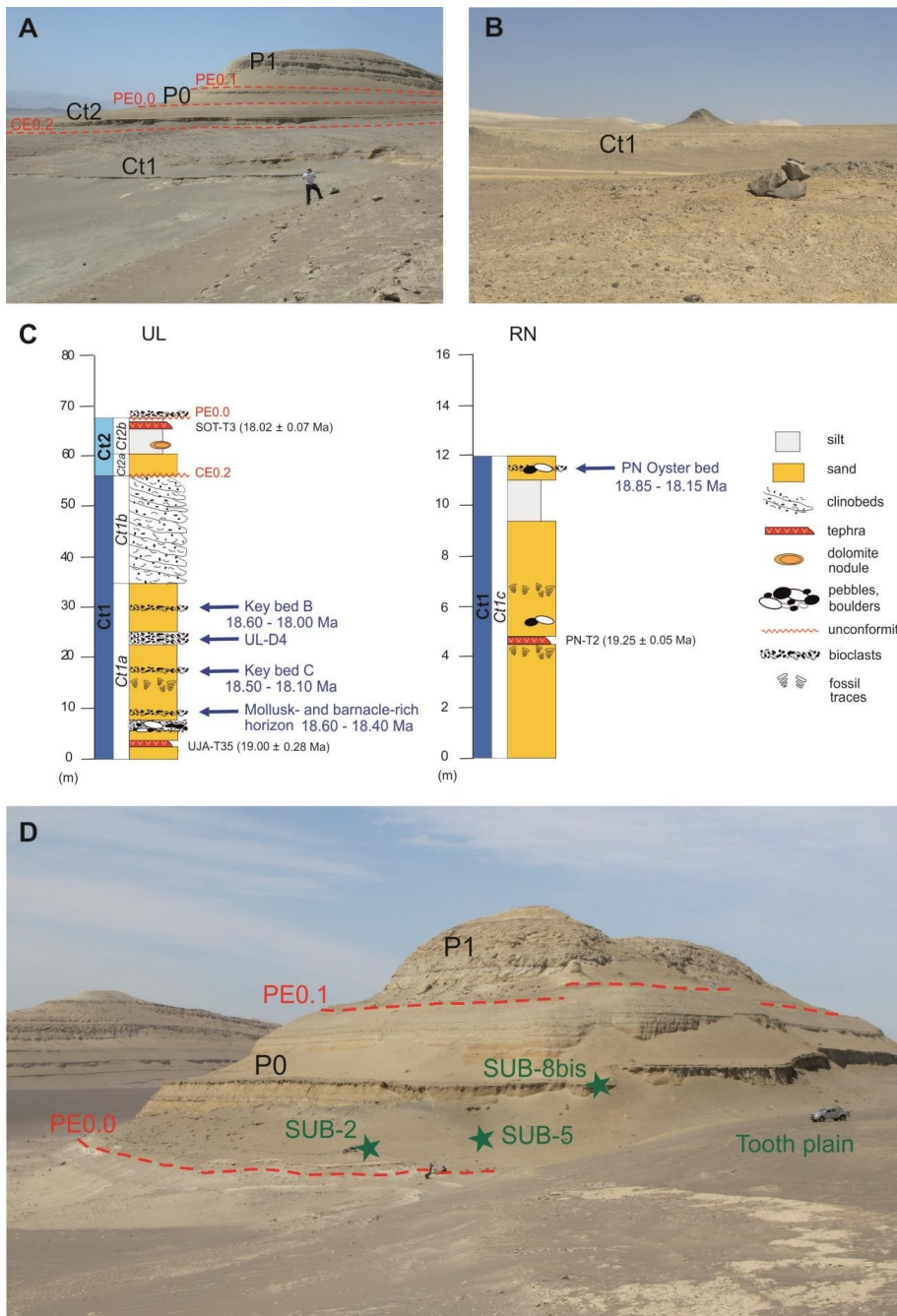


930

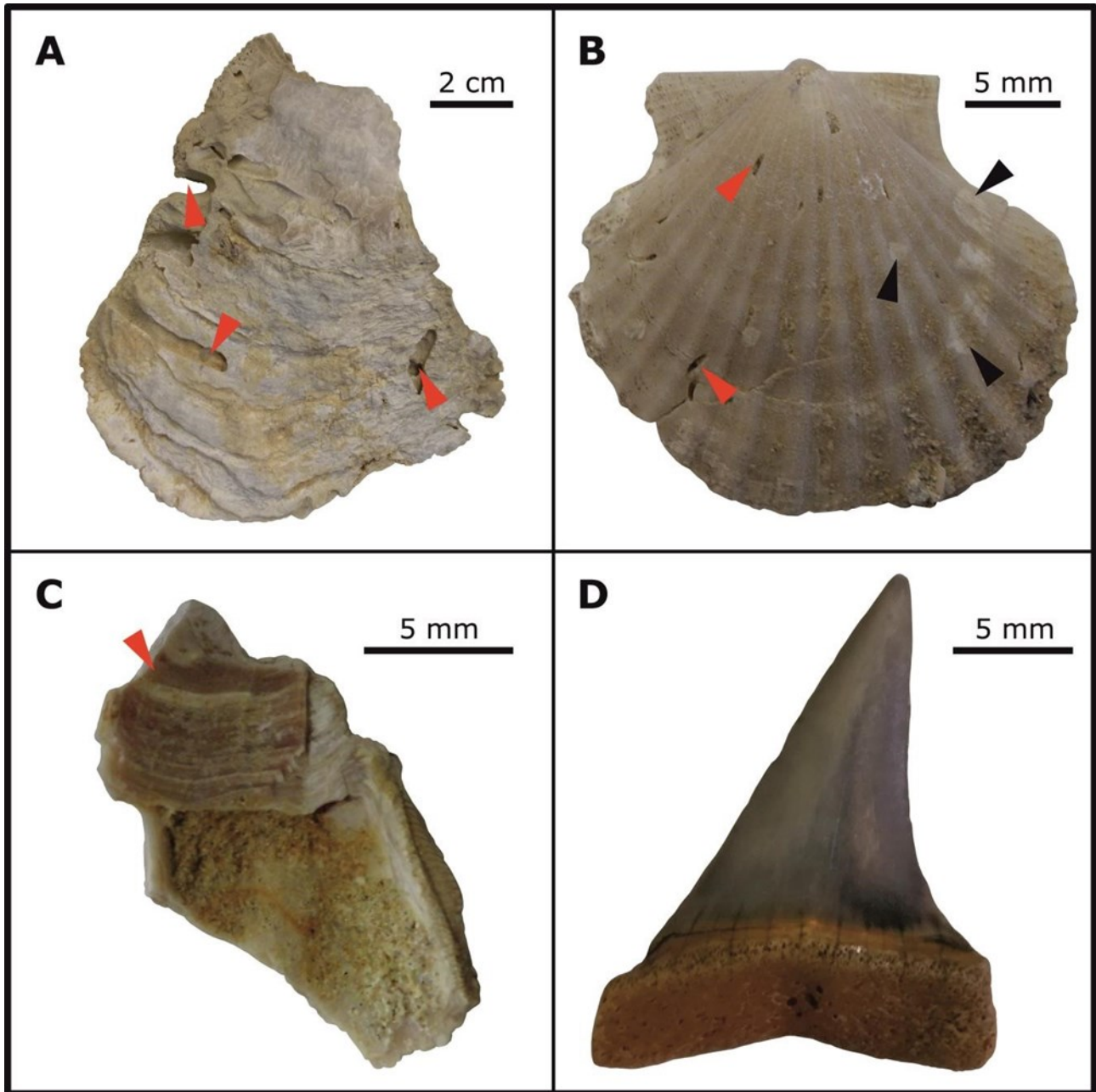
931 **Figure 2.** Satellite image and position of the localities of Cerro Submarino (), Ullujaya (), and Roca  
932 Negra () along the western side of the Ica River (Ica desert). Based on a Google Earth image (©  
933 2019 Maxar Technologies).

934





935  
 936 **Figure 3.** **A.** Field photo of the Chilcatay and Pisco strata at the locality of Ullujaya, **B.** Field photo  
 937 of the Chilcatay basal strata at the locality of Roca Negra. **C.** Schematic stratigraphic sections  
 938 measured at the Chilcatay outcrops of Ullujaya (UL) and Roca Negra (RN) that show the  
 939 stratigraphic position of i) the investigated beds and their  $^{87}\text{Sr}/^{86}\text{Sr}$  ages and ii) the ash layers with  
 940 the  $^{39}\text{Ar}-^{40}\text{Ar}$  ages obtained by Bosio et al. (in press). **D.** Field photo at Cerro Submarino, with the  
 941 location of the sampled beds (green stars) collected from the P0 sequence. The PE0.0 and PE0.1  
 942 unconformities are traced in red.

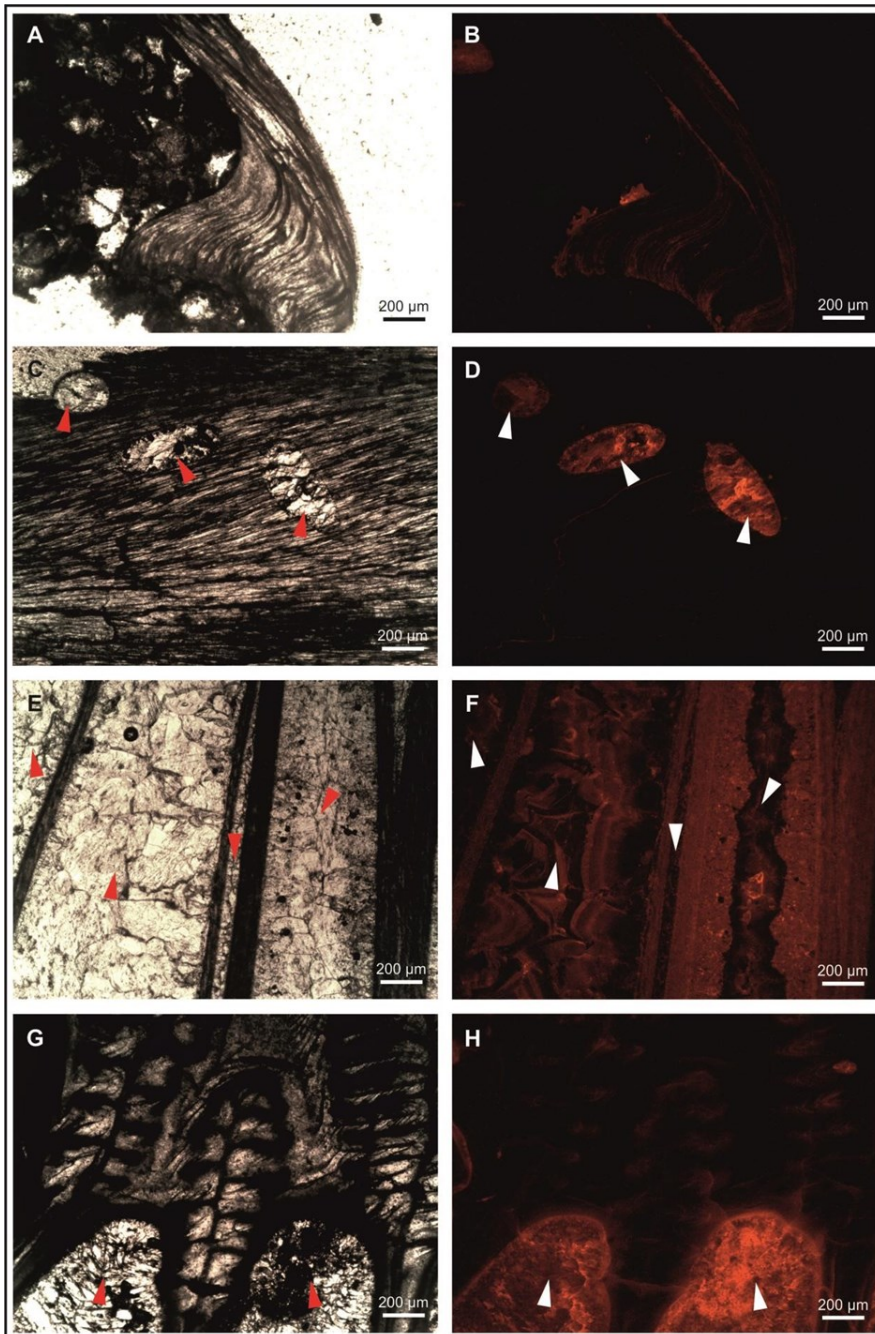


943

944 **Figure 4.** **A.** Oyster shell from the PN Oyster level in the Ct1 sequence at Roca Negra. Note the  
945 predation holes on the outer part of the shell pointed out by red arrows. **B.** Pectinid specimen from  
946 the mollusk- and barnacle-rich horizon in the Ct1 sequence at Ullujaya. Note the small drill holes  
947 (red arrows) and the barnacle attachment scars (i.e., *Anellusichnus*) (black arrows). **C.** Barnacle  
948 plate from the Key bed C in the Ct1 sequence at Ullujaya. Note the lamellar sheath (i.e., the  
949 thickened upper part of the inner wall pointed out by the red arrow) from which the SIS samples  
950 were taken. **D.** Tooth of *Cosmopolitodus hastalis* from the P0 sequence at Cerro Submarino.

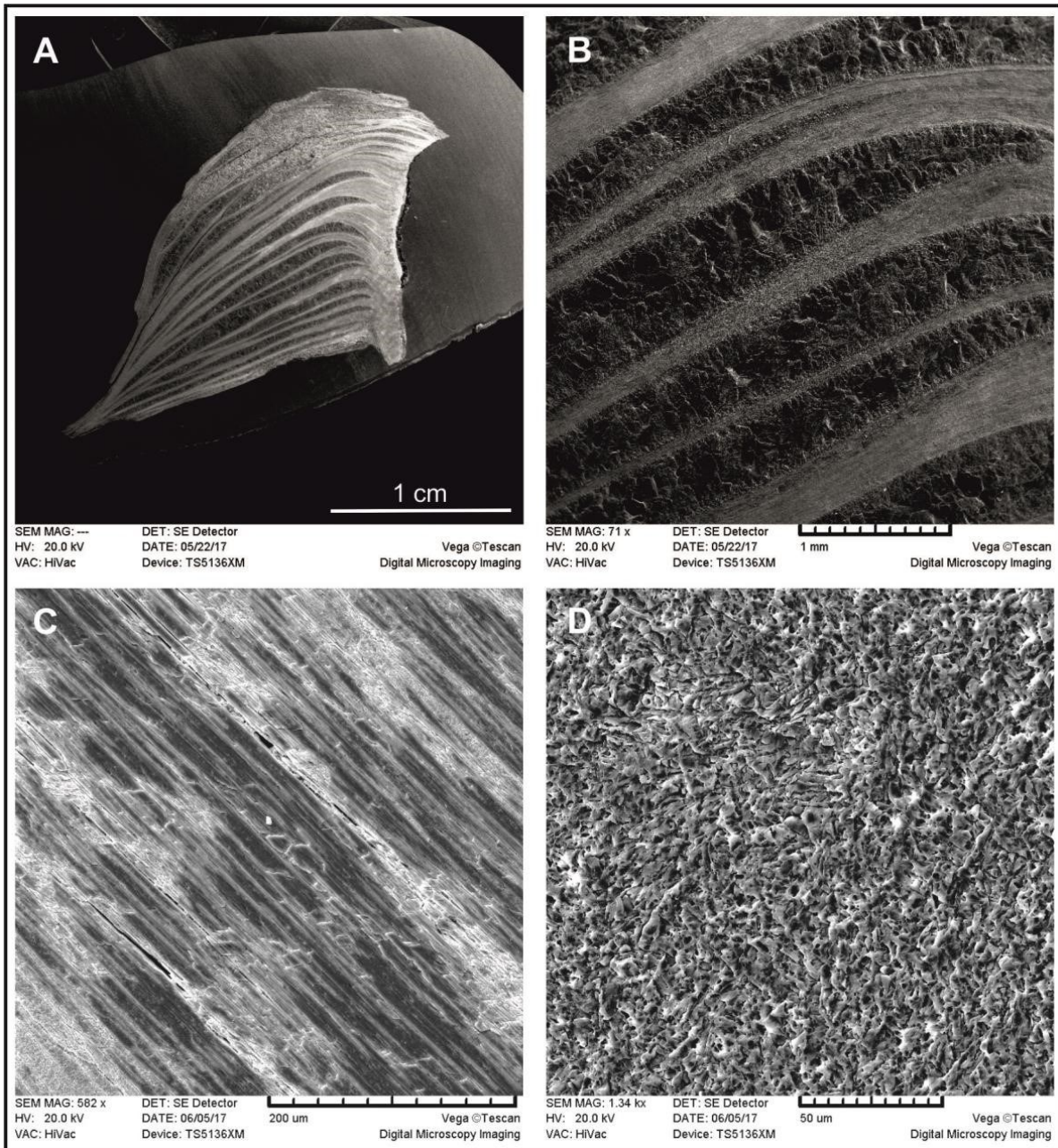
951





952

953 **Figure 5.** Transmitted light and cathodoluminescence microscopical photos. **A, B.** Pectinid shell  
954 with a homogenous luminescence. **C, D.** Oyster prismatic layer with a low and homogeneous  
955 luminescence, punctuated by microborings with a high luminescence (red and white arrows). **E, F.**  
956 A poorly preserved oyster shell characterized by an alternation of high luminescent layers of sparry  
957 calcite (red and white arrows). **G, H.** Transverse thin section of a barnacle shell showing tree-like  
958 interlaminar figures and the parietal tubes filled by diagenetic calcite with a high luminescence  
959 pointed out by red and white arrows.



960

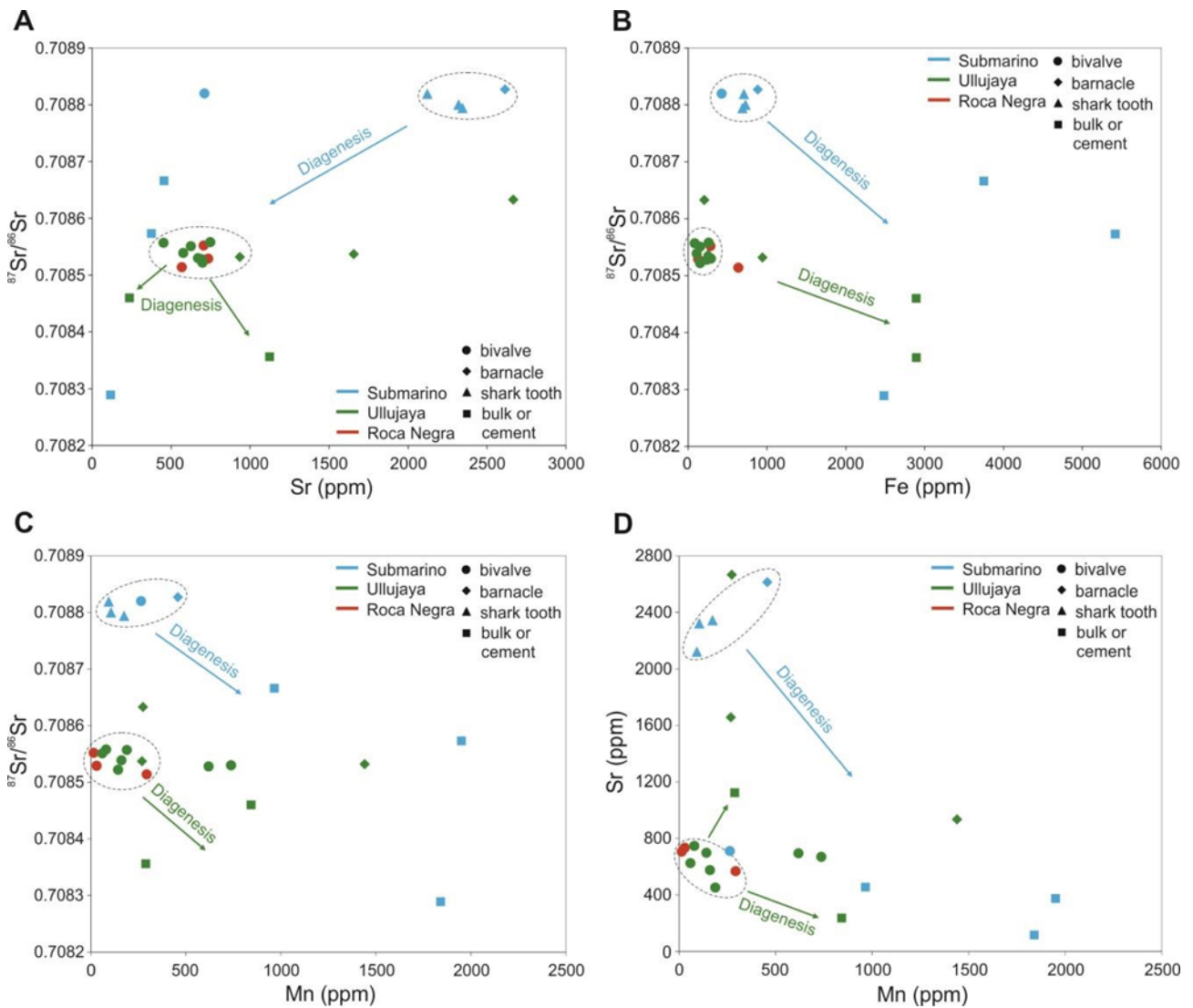
961 **Figure 6. A.** SE (Secondary Electron) image of an oyster cross-section. Note the alternation of  
962 different layers. **B.** Close-up of the oyster shell depicted in panel A. Note the alternation of  
963 prismatic layers (light grey) and sparry calcite layers (dark grey). **C.** SE image of a well-preserved  
964 prismatic layer of an oyster. **D.** SE image of a poorly preserved oyster shell exhibiting dissolution  
965 features as obliteration of the pristine prismatic texture and widespread, pervasive holes.

966

967

968

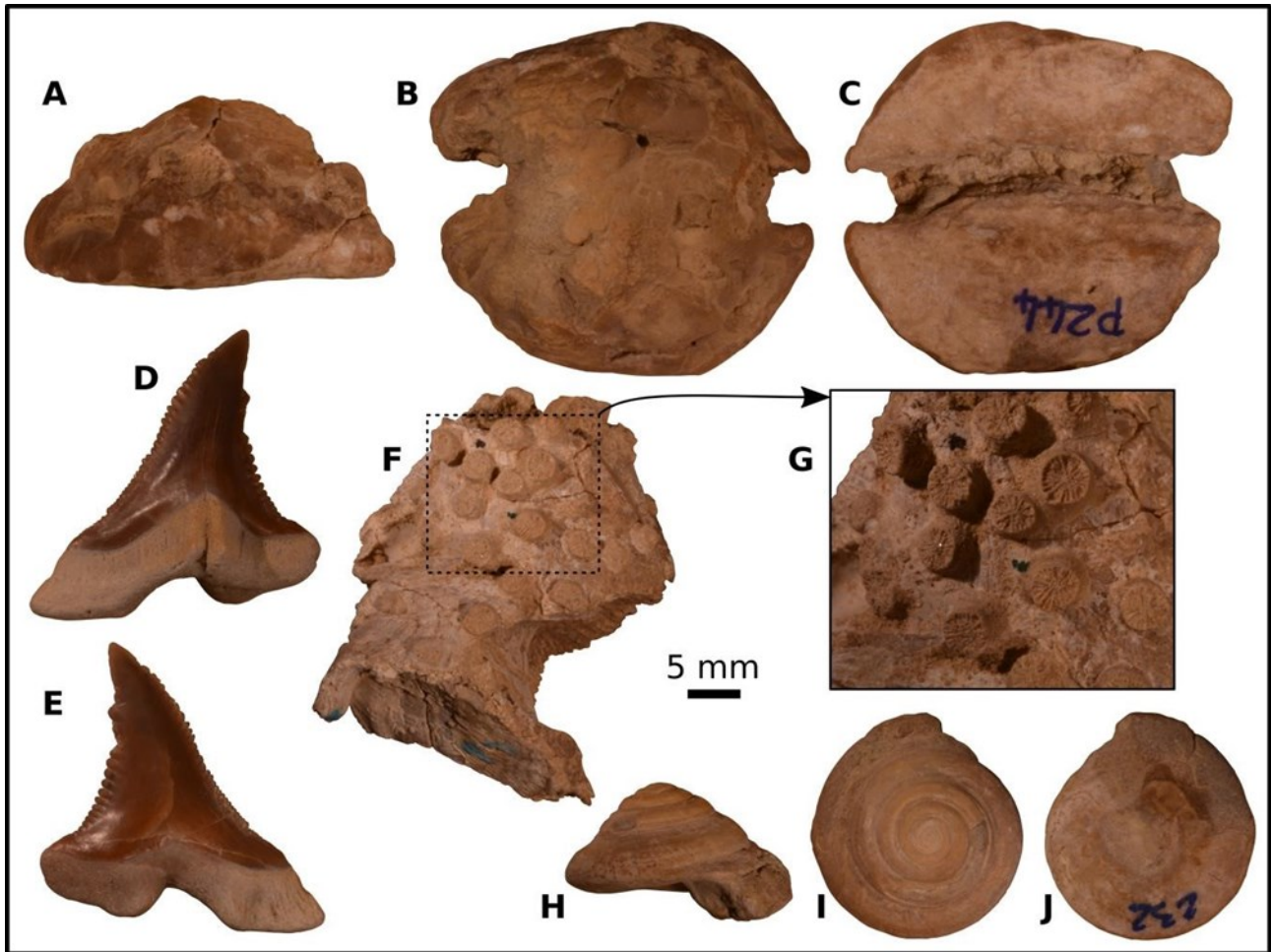




969

970 **Figure 7.** Diagenetic path diagrams, showing the major trends of diagenetic alteration in multi-  
 971 component plots. **A.**  $^{87}\text{Sr}/^{86}\text{Sr}$  ratio vs Fe concentration. **B.**  $^{87}\text{Sr}/^{86}\text{Sr}$  ratio vs Mn concentration.  
 972 Ellipses show well preserved (continuous line) and altered (dotted line) samples. Arrows indicate  
 973 trends of diagenetic alteration.

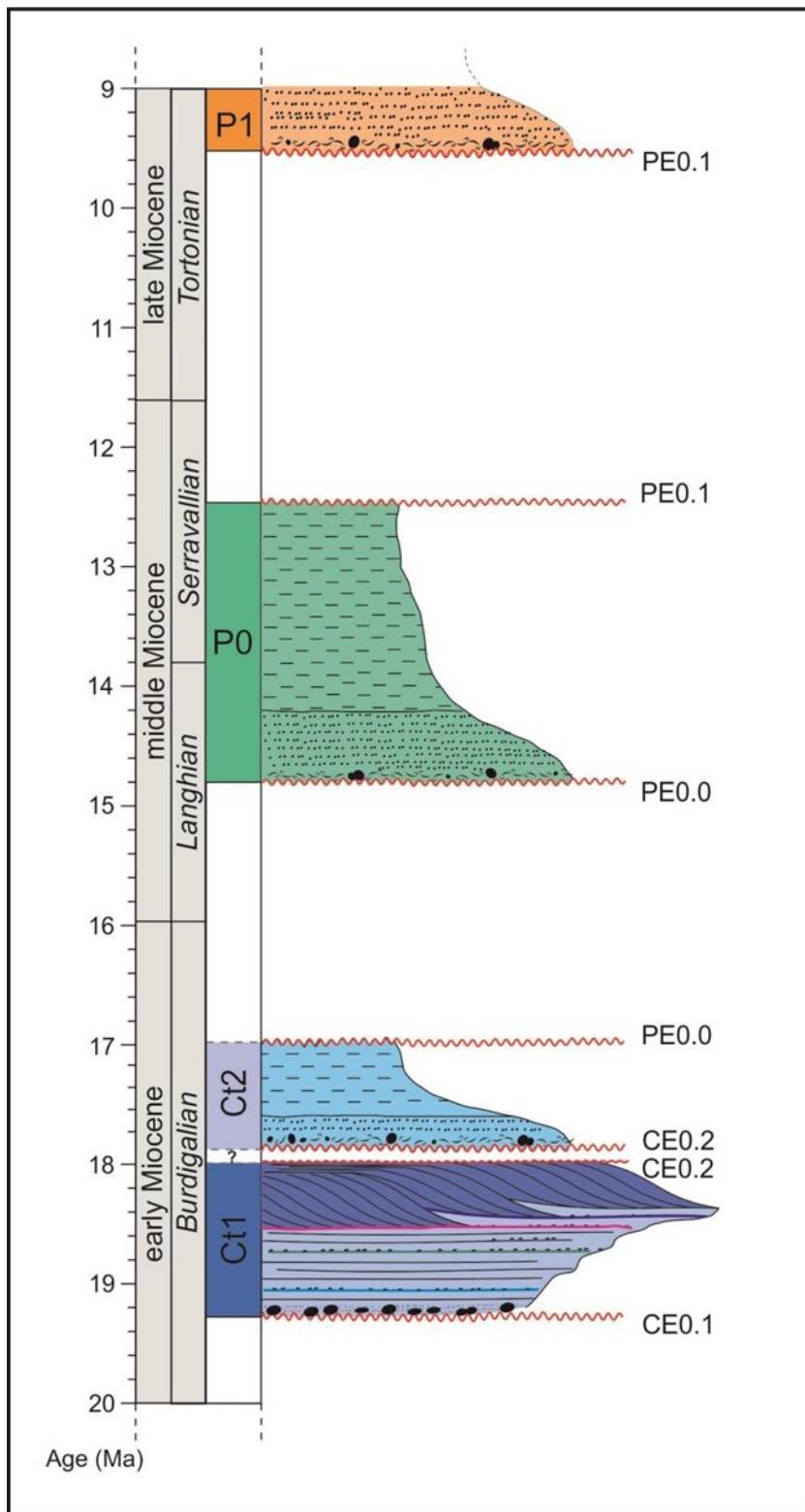
974



975

976 **Figure 8.** Fossils of warm-water taxa from the P0 sequence. **A, B, C.** Cypraeid specimen in lateral  
977 (A), dorsal (B), and apertural (C) views. **D, E.** Tooth of *Hemipristis serra* in lingual (A) and labial  
978 (B) views. **F.** Rhizangiid corallites encrusting a cluster of barnacle shells. **G.** Close-up of the  
979 corallites depicted in panel F. **H, I, J.** Architectonicid specimen in lateral (H), dorsal (I), and ventral  
980 (J) views.

981



982

983 **Figure 9.** Schematic chronostratigraphic section of the Chilcatay (Ct1 and Ct2) and Pisco (P0 and  
984 P1) sequences according to Strontium Isotope Stratigraphy.

985

986

987 **Table captions****Table 1**

Formation	Sequence	Locality	Stratigraphic level	Samples	Description	Measured $^{87}\text{Sr}/^{86}\text{Sr}$	$\pm 2\sigma$ mean	Corrected $^{87}\text{Sr}/^{86}\text{Sr}$			
Pisco Fm	P0	Cerro Submarino	SUB-8bis	SUB-8bis1	Barnacle sheath	0.708811	0.000005	0.708827			
				SUB-8bis2	Bulk cemented sediment	0.708273	0.000005	0.708289			
				SUB-8bis3	Recrystallized bivalve shell	0.708650	0.000005	0.708666			
					SUB-5	SUB-5	Ostreidae specimen	0.708804	0.000005	0.708820	
					SUB-2	SUB-2	Calcite nodule	0.708557	0.000005	0.708573	
					Tooth plain	Tooth 1	Shark tooth: <i>Cosmopolitodus hastalis</i>	0.708803	0.000005	0.708819	
						Tooth 2	Shark tooth: <i>Cosmopolitodus hastalis</i>	0.708778	0.000005	0.708794	
						Tooth 3	Shark tooth: <i>Isurus oxyrinchus</i>	0.708784	0.000005	0.708800	
			Chilcatay Fm	Ct1	Ullujaya	Key bed B	UJA-2a	Ostreidae specimen	0.708541	0.000005	0.708557
UJA-2b	Ostreidae specimen	0.708523					0.000005	0.708539			
		UL-D4					UL-D4a	Ostreidae specimen	0.708506	0.000004	0.708522
						UL-D4b	Barnacle sheath	0.708617	0.000005	0.708633	
						UL-D4c	Bulk cemented sediment	0.708444	0.000005	0.708460	
		Key bed C				UJA-LIVC1	Ostreidae specimen	0.708535	0.000005	0.708551	
						UJA-LIVC2	Bulk cemented sediment	0.708340	0.000005	0.708356	
						UJA-LIVC3	Ostreidae specimen	0.708542	0.000005	0.708558	
						UJA-LIVC4	Barnacle sheath	0.708521	0.000005	0.708537	
		Mollusc- and barnacle-rich horizon				UL-LIVa	Barnacle sheath	0.708516	0.000005	0.708532	
						UL-LIVb	Pectinidae specimens	0.708512	0.000005	0.708528	
						UL-LIVd	Pectinidae specimen	0.708514	0.000005	0.708530	
		Roca Negra				PN Oyster bed	PN-OST	Ostreidae specimen	0.708498	0.000005	0.708514
							PN-GIO1	Ostreidae specimen	0.708513	0.000007	0.708529
							PN-GIO2	Ostreidae specimen	0.708536	0.000005	0.708552

988

989 **Table 1.** Sample list and description, with locality and stratigraphic data, reporting  $^{87}\text{Sr}/^{86}\text{Sr}$   
990 measured values and standard deviation, with  $^{87}\text{Sr}/^{86}\text{Sr}$  values corrected for the difference between  
991 the USGS EN-1 value used for the compilation of the reference curve (McArthur et al., 2012) and  
992 the USGS EN-1 Bochum mean value.

	Stratigraphic level	<i>minus 2 s.e.</i>	$^{87}\text{Sr}/^{86}\text{Sr}$ mean value	<i>plus 2 s.e.</i>	Maximum age (Ma)	Preferred age (Ma)	Minimum age (Ma)
<b>P0</b>	Lower P0	0.708799	0.708812	0.708825	14.80	13.45	12.45
	Key bed B	0.708530	0.708548	0.708566	18.60	18.30	18.00
<b>Ct1</b>	Key bed C	0.708536	0.708549	0.708561	18.50	18.30	18.10
	Mollusk- and barnacle-rich horizon	0.708528	0.708530	0.708532	18.60	18.50	18.40
	PN Oyster bed	0.708510	0.708532	0.708554	18.85	18.50	18.15

993

994 **Table 2.**  $^{87}\text{Sr}/^{86}\text{Sr}$  ages for the Ct1 and P0 sequences, calculated from the LOWESS Table 5  
995 (McArthur et al., 2012).